Title: Ground- and excited-state properties of Re(I) carbonyl complexes - effect of triimine ligand core and appended heteroaromatic groups

Author: Katarzyna Choroba, Sonia Kotowicz, Anna Maroń, Anna Świtlicka, Agata Szłapa-Kula, Ewa Schab-Balcerzak, Barbara Machura i in.

Citation style: Choroba Katarzyna, Kotowicz Sonia, Maroń Anna, Świtlicka Anna, Szłapa-Kula Agata, Schab-Balcerzak Ewa, Machura Barbara i in. (2021). Ground- and excited-state properties of Re(I) carbonyl complexes - effect of triimine ligand core and appended heteroaromatic groups. "Dyes and Pigments" (Vol. 192, (2021) art. no. 109472), doi 10.1016/j.dyepig.2021.109472

Dyes and Pigments 192 (2021) 109472

Ground- and excited-state properties of Re(I) carbonyl complexes – Effect of triimine ligand core and appended heteroaromatic groups

Katarzyna Choroba [a], Sonia Kotowicz [a], Anna Maroń [a], Anna Świtlicka [a], Agata Szłapa-Kula [a], Mariola Siwy [b], Justyna Grzelak [c], Karolina Sulowska [c], Sebastian Maćkowski [c], Ewa Schab-Balcerzak [a,b,**], Barbara Machura [a,*]

[a] Institute of Chemistry, University of Silesia, 9th Szkolna St., 40-006, Katowice, Poland
[b] Centre of Polymer and Carbon Materials, Polish Academy of Sciences, 34th M. Curie-Sklodowska St., 41-819, Zabrze, Poland
[c] Institute of Physics, Faculty of Physics, Astronomy and Informatics, Nicolaus Copernicus University, 5th Grudziadzka St., 87-100, Torun, Poland

ARTICLE INFO

Keywords:
Re(I) carbonyl complexes
Triimine ligands
Photoluminescence
Electroluminescence
Femtosecond transient absorption spectroscopy

ABSTRACT

In this work, a series of six rhenium(I) complexes bearing 2,2′:6′,2″-terpyridine (*terpy*), 2,6-di(thiazol-2-yl)pyridine (*dtpy*), and 2,6-di(pyrazin-2-yl)pyridine (*dppy*) with appended quinolin-2-yl and N-ethylcarbazol-3-yl groups were prepared and spectroscopically investigated to evaluate the photophysical consequences of both the trisheterocyclic core (*terpy, dtpy* and *dppy*) and the heterocyclic substituent. The [ReCl(CO)$_3$(L^n-κ^{2}N)] complexes are regarded as ideal candidates for getting structure–property relationships, while *terpy*-like framework represents an excellent structural backbone for structural modifications. The replacement of the peripheral pyridine rings of 2,2′:6′,2″-terpyridine by thiazoles and pyrazines resulted in a significant red-shift of the absorption and emission of [ReCl(CO)$_3$(L^n-κ^{2}N)] due to stabilization of the ligand-centred LUMO orbital. Both quinoline and N-ethylcarbazole are extended π-conjugation organic chromophores, but they differ in electron-donating abilities. The low-energy absorption band of Re(I) complexes with the triimine ligands bearing quinolin-2-yl group was contributed by the metal-to-ligand charge-transfer (MLCT) electronic transitions. The introduction of electron-donating N-ethylcarbazol-3-yl substituent into the triimine acceptor core resulted in the change of the character of the HOMO of Re(I) complexes and a significant increase of molar absorption coefficients of the long-wavelength absorption, which was assigned to a combination of ^{1}MLCT and ^{1}ILCT (intraligand charge-transfer) transitions. Regardless of the appended heteroaromatic group, the emitting excited state of Re(I) *terpy*-based complexes was demonstrated to have predominant ^{3}MLCT character, as evidenced by comprehensive studies including static and time-resolved emission spectroscopy along with ultrafast transient absorption measurements. The diodes with Re(I) complexes dispersed molecularly in a PVK:PBD matrix were emissive and effects of the complex structure on colour of emitted light and its intensity was pronounced.

1. Introduction

Transition metal coordination compounds incorporating 2,2′:6′,2″-terpyridines substituted in 4-position of the central pyridine ring (4′-R-*terpy*) have attracted considerable attention, and they have been subject of intensive investigations in view of their optical, electrochemical, luminescent, magnetic, catalytic, and therapeutic properties which are relevant for potential applications in various areas including catalysis [1–4], solar energy conversion [5–7], molecular magnetism [8–10], optoelectronic devices [11–13], sensors [14,15] and medicinal chemistry [16–21]. High stability of these systems is attributed to the thermodynamic chelate effect and σ-donor/π-acceptor character of the metal-to-ligand bond. 2,2′:6′,2″-Terpyridine core commonly acts as a tridentate ligand [4,22,23], but reports concerning bidentate fashion of 4′-R-*terpy* can be also found, especially for Pt(IV) [24–27], Re(I) [28–33] and W(0) [34]. Although a metal ion seems to have a crucial role in determining the properties of resulting coordination compounds, functionality of 2,2′:6′,2″-terpyridine compounds bearing the same metal may be also widely tuned by introduction of electron donating and withdrawing substituents into *terpy* skeleton [23,35–38]. Another

* Corresponding author. Institute of Chemistry, University of Silesia, 9th Szkolna St., 40-006, Katowice, Poland.
** Corresponding author. Institute of Chemistry, University of Silesia, 9th Szkolna St., 40-006, Katowice, Poland.
E-mail addresses: ewa.schab-balcerzak@us.edu.pl (E. Schab-Balcerzak), barbara.machura@us.edu.pl (B. Machura).

https://doi.org/10.1016/j.dyepig.2021.109472
Received 24 February 2021; Received in revised form 28 April 2021; Accepted 10 May 2021
Available online 14 May 2021

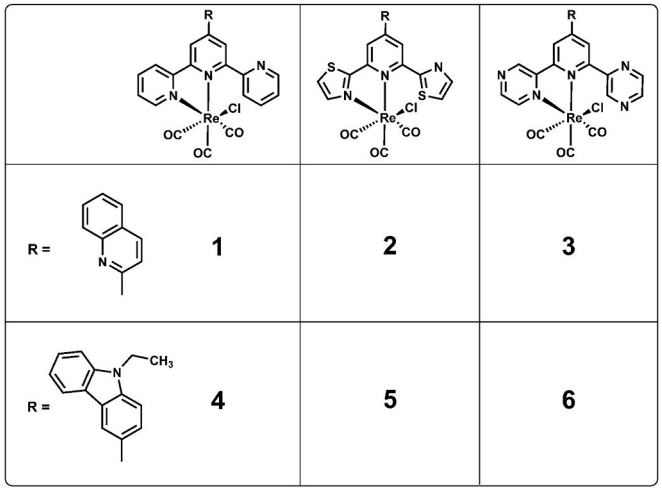

Scheme 1. Re(I) carbonyl complexes under study.

interesting approach of modifying the physical properties of these systems concerns substitution of peripheral pyridine rings of 2,2′:6′, 2″-terpyridine by different heterocycles (triazoles [39,40], pyrazoles [41,42], triazines [43], dihydrooxazoles [44], benzimidazoles [45], thiazoles [31,45,46], pyrazines [47]), which leads to numerous *terpy*--like ligands widely used for design of new coordination compounds with respectively tuned properties.

In the present paper, a series of rhenium carbonyls bearing 2,2′:6′,2″-terpyridine, 2,6-di(thiazol-2-yl)pyridine, and 2,6-di(pyrazin-2-yl)pyridine functionalized with quinolin-2-yl and N-ethylcarbazol-3-yl pendant substituents have been synthesized and investigated experimentally and theoretically (Scheme 1).

The [ReCl(CO)$_3$(L^n-κ^{2}N)] complexes are regarded as ideal candidates for getting structure–property relationships. The nature of the excited-states of [ReCl(CO)$_3$(L^n-κ^{2}N)] and thus their photophysical properties are impacted by the interplay between relative energy levels of the metal and ligand orbitals, while *terpy*-like framework represents an ideal structural backbone for modifications. In these studies, we focus on an exploration of the impact of the trisheterocyclic core (*terpy, dtpy* and *dppy*) and heterocyclic substituent on the ground- and excited-state properties of [ReCl(CO)$_3$(L^n-κ^{2}N)]. Noteworthy, carbazole is a molecular unit of outstanding importance in organic materials due to electron donating properties and excellent hole-transporting abilities [48]. Introduced into the trisheterocyclic acceptor core, directly [49–51] or attached through a phenylene bridge [52,53], it can give rise to intra-ligand charge-transfer (ILCT) transitions from donor orbital localized on the electron-rich group to triimine-based π*acceptor orbital. Likewise as N-ethylcarbazole, quinoline is an extended π-conjugation organic chromophore of great importance in view of potential OLED applications [54,55], but it shows significantly weaker electron-donating ability. Therefore, it is expected to favour metal-ligand charge transfer (MLCT) excited state of [ReCl(CO)$_3$(L^n-κ^{2}N)] [56–59]. The complex **5**, reported in Ref. [32] has been included in the current work for comparison purpose.

The energies and character of the electronic transitions that occur in these systems were investigated with electrochemistry, absorption and emission spectroscopies, as well as theoretically using DFT calculations at the PBE1PBE/DEF2–TZVPD/DEF2–TZVP level. Also, the capacity of the obtained compounds for electroluminescence was studied.

2. Experimental section

2.1. Materials

Re(CO)$_5$Cl (Sigma Aldrich), poly(9-vinylcarbazole) PVK (M_n = 25 000–50 000; Sigma Aldrich), 2-(4-tert-butylphenyl)-5-(4-biphenylyl)-1,3,4-oxadiazole PBD (Sigma Aldrich), poly(3,4-(ethylenedioxy)thiophene):poly-(styrenesulfonate) PEDOT:PSS (0.1–1.0 S/cm), and substrates with pixilated ITO anodes (Ossila), as well as all solvents for syntheses (of reagent grade) and for spectroscopic studies (of HPLC grade) were commercially available and used without further purification. All the ligands (L^1–L^6) were prepared according to the method reported previously [60–64], and detailed synthetic procedure was provided in Electronic Supplementary Information (ESI). The films and blends with PVK:PBD (50:50 wt %) on a glass substrate as well as all the devices with the configurations: ITO:PEDOT:PSS/complex/Al and ITO:PEDOT:PSS/PVK:PBD:complex/Al with 15, 2 and 1 wt % Re(I) carbonyl complex content in blend were prepared according to the method reported in our previous works [29–33] and additionally are briefly described in ESI.

2.2. Preparation of [ReCl(CO)$_3$(L^n-κ^{2}N)] (1–6)

Re(I) carbonyl complexes were prepared using the procedure given in our previous works [31,32]: [Re(CO)$_5$Cl] (0.10 g, 0.27 mmol) and suitable L^n ligand (0.27 mmol) were dissolved in argon-saturated acetonitrile (60 mL), and the reaction solution was placed in Teflon-lined hydrothermal synthesis autoclave. The reactor was heated to 150 °C for 20 h, kept in that temperature for 30 h, and then gradually cooled to room temperature over the next 30 h. The resulting powders (**1**, **4** and **5**) or crystalline solids (**2**, **3** and **6**) were collected by filtration, recrystallized in chloroform, washed with diethyl ether and air-dried.

2.2.1. [ReCl(CO)$_3$(4′-(quinolin-2-yl)-2,2′:6′,2″-terpyridine-κ^{2}N)], 1

Yield: 80%. IR (KBr, cm^{-1}): 2019(vs), 1911(vs) and 1882(vs) ν(C≡O); 1614(m), 1589(m) and 1568(w) ν(C=N) and ν(C=C). **^{1}H NMR** (600 MHz, DMSO) δ 9.50 (s, 1H), 9.14 (d, *J* = 8.2 Hz, 1H), 9.11 (d, *J* = 5.3 Hz, 1H), 8.85 (d, *J* = 4.5 Hz, 1H), 8.74–8.70 (m, *J* = 5.1 Hz, 3H), 8.44 (t, *J* = 7.9 Hz, 1H), 8.23 (d, *J* = 8.5 Hz, 1H), 8.13 (d, *J* = 8.1 Hz, 1H), 8.10 (t, *J* = 7.7 Hz, 1H), 7.95 (d, *J* = 7.7 Hz, 1H), 7.89 (t, *J* = 7.7 Hz, 1H), 7.82 (t, 1H), 7.74 (t, *J* = 7.5 Hz, 1H), 7.67 (t, 1H). **^{13}C NMR** (100 MHz, DMSO) δ 198.2, 194.8, 191.4, 162.2, 158.3, 158.0, 156.6, 153.3, 151.9, 149.9, 149.5, 148.0, 140.6, 138.6, 137.5, 131.2, 130.1, 128.7, 128.7, 128.5, 128.1, 126.0, 125.7, 125.6, 125.0, 121.4, 120.1. Anal. calc. found: C 46.46; H 2.36; N 7.83%; molecular formula [ReCl(CO)$_3$(N$_4$C$_{24}$H$_{16}$)]·1/3(CHCl$_3$) requires C 46.51; H 2.33; N 7.94%. DSC: T_m = 304 °C.

2.2.2. [ReCl(CO)$_3$(4-(quinolin-2-yl)-2,6-di(thiazol-2-yl)pyridine-κ^{2}N)], 2

Yield: 68%. IR (KBr, cm^{-1}): 2021(vs), 1924(vs) and 1893(vs) ν(C≡O); 1618(m) and 1608(w) ν(C=N) and ν(C=C). ^{1}H NMR (400 MHz, Acetone) δ 9.34 (d, *J* = 1.6 Hz, 1H), 8.85 (d, *J* = 1.6 Hz, 1H), 8.66 (d, *J* = 8.6 Hz, 1H), 8.61 (d, *J* = 8.7 Hz, 1H), 8.42 (d, *J* = 3.3 Hz, 1H), 8.31 (d, *J* = 3.3 Hz, 1H), 8.27 (d, *J* = 8.3 Hz, 1H), 8.20 (d, *J* = 3.2 Hz, 1H), 8.14 (d, *J* = 3.2 Hz, 1H), 8.11 (d, *J* = 8.0 Hz, 1H), 7.92 (t, *J* = 7.6 Hz, 1H), 7.76 (t, *J* = 7.5 Hz, 1H). **^{13}C NMR** not recorded due to insufficient complex solubility. Anal. calc. found: C 39.09; H 1.76; N 7.86; S 8.61%; molecular formula [ReCl(CO)$_3$(N$_4$S$_2$C$_{20}$H$_{12}$)]·1/3(CHCl$_3$) requires C 39.03; H 1.73; N 7.80; S 8.93%. DSC: T_m = 171, 190, 206 °C (I heating scan); T_g = 182 °C (II heating scan).

2.2.3. [ReCl(CO)$_3$(4-(quinolin-2-yl)-2,6-di(pyrazin-2-yl)pyridine-κ^{2}N)], 3

Yield: 52%. IR (KBr, cm^{-1}): 2027(vs), 1936(s) and 1914(vs) ν(C≡O); 1620(m), 1594(w) ν(C=N) and ν(C=C). **^{1}H NMR** (400 MHz, DMSO) δ 10.42 (s, 1H), 9.75 (s, 1H), 9.20 (s, 1H), 9.19 (d, *J* = 2.5 Hz, 1H), 9.03 (d, *J* = 2.9 Hz, 1H), 8.97 (s, 2H), 8.90 (s, 1H), 8.75 (s, 2H), 8.25 (d, *J* = 8.4 Hz, 1H), 8.14 (d, *J* = 8.0 Hz, 1H), 7.91 (t, *J* = 7.4 Hz, 1H), 7.76 (t, *J* = 7.4 Hz, 1H). **^{13}C NMR** (100 MHz, DMSO) δ 196.4, 194.4, 189.5, 159.0, 156.0, 153.5, 151.0, 150.8, 149.3, 148.1, 147.5, 147.1, 146.0, 145.4, 144.3, 138.2, 130.8, 129.6, 128.3, 128.3, 128.0, 125.7, 122.0, 119.7.

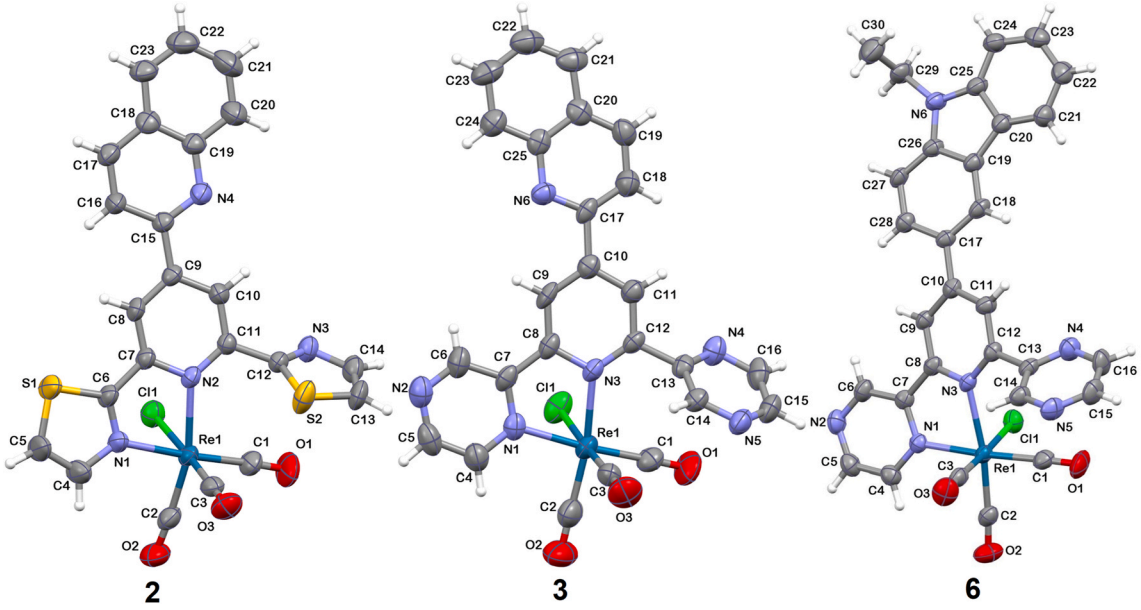

Fig. 1. Molecular structures of **2**, **3** and **6** together with the atom numbering. Displacement ellipsoids are drawn at 50% probability level.

Table 1
Cyclic voltammetry data of 1–6.

Complex	E_{red} [V]	$E_{red(onset)}$ [V]	E_{ox} [V]	$E_{ox(onset)}$ [V]	EA [eV]	IP [eV]	E_g [eV]	E_g^{opt} [eV]
1	−1.78[b]	−1.65	0.75	0.57	−3.45	−5.67	2.22	1.86
2	−1.64[b]	−1.51	0.83	0.66	−3.59	−5.76	2.17	1.64
3	−1.59[a]	−1.36	1.01	0.77	−3.74	−5.87	2.13	1.68
4	−1.85	−1.73	0.75	0.65	−3.37	−5.75	2.38	1.97
5	−1.63	−1.53	0.87	0.77	−3.57	−5.87	2.30	1.74
6	−1.49	−1.38	0.91	0.78	−3.72	−5.88	2.16	1.72

IP = −5.1–$E_{ox(onset)}$, EA = −5.1–$E_{red(onset)}$, E_g = $E_{ox(onset)}$–$E_{red(onset)}$.
[a] Irreversible.
[b] Quasi-reversible. $E_g^{opt} = 1241/\lambda_{em}$.

Table 2
Spectral parameters of the Re(I) complexes **1**–**6**.

Complex	Medium	Absorption wavelength [nm] (Molar absorption coefficient × 10^4 [$dm^3 \cdot mol^{-1} \cdot cm^{-1}$])
1	CH_3CN	385 (0.6), 318 (2.7), 266 (4.2)
	$CHCl_3$	404 (0.6), 321 (2.8), 266 (3.7)
	film	400, 326
2	CH_3CN	397 (0.5), 321 (2.2), 269 (4.3)
	$CHCl_3$	418 (0.4), 331 (2.2), 268 (2.1)
	film	415, 343
3	CH_3CN	407 (0.5), 325 (3.1), 270 (3.5), 254 (3.3)
	$CHCl_3$	432 (0.4), 329 (2.83), 261 (2.8)
	film	415, 339
4	CH_3CN	391 (2.5), 302 (3.9), 286 (4.2), 230 (5.7)
	$CHCl_3$	397 (2.2), 304 (3.7), 292 (4.0)
	film	420, 309
5[a]	CH_3CN	411 (1.6), 318 (2.2), 290 (2.2), 262 (2.2), 245 (2.8), 236 (3.1), 229 (3.1)
	$CHCl_3$	418 (1.8), 325 (2.9), 293 (3.0), 266 (3.1), 246 (3.8)
	film	437, 326
6	CH_3CN	412 (1.7), 313 (3.3), 285 (3.6), 232 (4.7)
	$CHCl_3$	426 (1.6), 316 (3.1), 290 (3.1)
	film	446, 340

[a] data for complex **5** taken from Ref. [32].

Anal. calc. found: C 44.61; H 2.16; N 12.72%; molecular formula [ReCl$(CO)_3(N_6C_{22}H_{14})$] requires: C 44.94; H 2.11; N 12.58% DSC: T_m = 308 °C.

2.2.4. [ReCl$(CO)_3$(4′-(N-ethylcarbazol-3-yl)-2,2′:6′,2″-terpyridine-κ^2N)], 4

Yield: 74%. IR (KBr, cm^{-1}): 2018(vs), 1907(vs) and 1889(vs) ν(C≡O); 1610(m) and 1594(m) ν(C=N) and ν(C=C). **^{1}H NMR** (600 MHz, DMSO) δ 9.20 (d, *J* = 1.4 Hz, 1H), 9.16 (d, *J* = 8.3 Hz, 1H), 9.14 (d, *J* = 1.6 Hz, 1H), 9.08 (d, *J* = 4.9 Hz, 1H), 8.83 (d, *J* = 4.4 Hz, 1H), 8.41 (t, 1H), 8.39–8.32 (m, 3H), 8.08 (t, *J* = 7.7 Hz, 1H), 7.94 (d, *J* = 7.7 Hz, 1H), 7.84 (d, *J* = 8.7 Hz, 1H), 7.79 (t, 1H), 7.70 (d, *J* = 8.2 Hz, 1H), 7.65 (t, *J* = 6.9 Hz, 1H), 7.54 (t, 1H), 7.30 (t, *J* = 7.5 Hz, 1H), 4.54 (q, *J* = 7.0 Hz, 2H), 1.37 (t, *J* = 7.1 Hz, 3H). **^{13}C NMR** (126 MHz, DMSO) δ 198.4, 195.0, 191.6, 161.7, 158.6, 157.4, 157.0, 153.2, 152.0, 149.7, 141.6, 140.7, 140.4, 137.4, 127.8, 127.0, 126.0, 125.8, 125.6, 125.4, 125.3, 124.0, 123.6, 122.9, 121.4, 121.0, 120.4, 120.0, 110.4, 110.2, 37.7, 14.3. Anal. calc. found: C 52.56; H 2.86; N 7.78%; molecular formula [ReCl$(CO)_3(N_4C_{29}H_{22})$] requires: C 52.49; H 3.03; N 7.65%. DSC: T_m = 327 °C.

2.2.5. [ReCl$(CO)_3$(4-(N-ethylcarbazol-3-yl)-2,6-di(thiazol-2-yl)pyridine-κ^2N)], 5

Reported previously in Ref. [32]. Yield: 70%. IR (KBr, cm-1): 2020 (vs), 1917(vs) and 1889(vs) ν(C≡O); 1609(m) and 1590(s) ν(C=N) and ν(C=C). **^{1}H NMR** (400 MHz, Acetone) δ 9.09 (d, *J* = 1.6 Hz, 1H), 8.94 (d, *J* = 1.8 Hz, 1H), 8.40 (d, *J* = 1.8 Hz, 1H), 8.38 (d, *J* = 3.3 Hz, 1H), 8.29 (t, 2H), 8.26 (d, *J* = 3.3 Hz, 1H), 8.17 (d, *J* = 3.2 Hz, 1H), 8.09 (d, *J* = 3.2 Hz, 1H), 7.82 (d, *J* = 8.7 Hz, 1H), 7.68 (d, *J* = 8.3 Hz, 1H), 7.56 (t, *J* = 7.6 Hz, 1H), 7.31 (t, *J* = 7.5 Hz, 1H), 4.59 (q, *J* = 7.2 Hz, 2H), 1.48 (t,

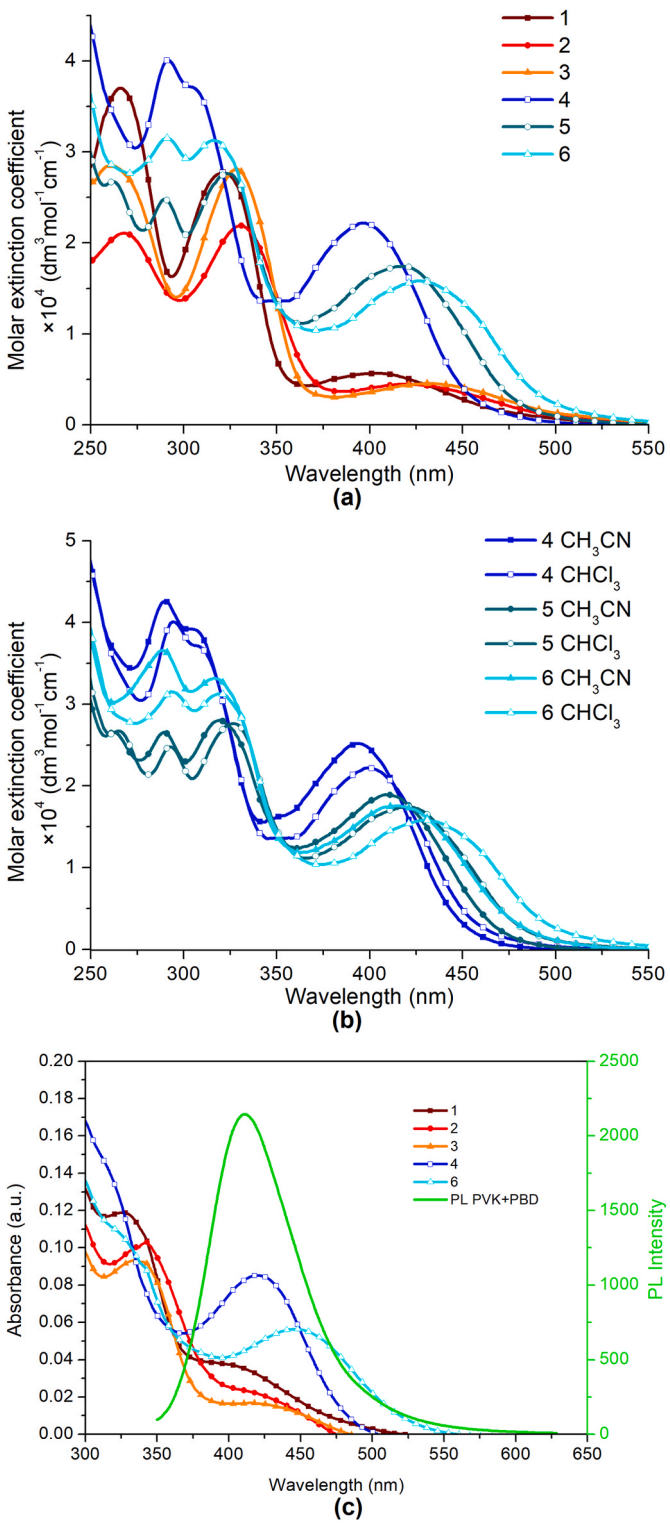

Fig. 2. UV–Vis spectra of **1**–**6** in $CHCl_3$ (a); Impact of solvent polarity on the UV–Vis spectra of **4**–**6** (b); UV–Vis spectra of **1**–**4** and **6** in film and emission spectrum of PVK:PBD (c).

J = 7.2 Hz, 3H). **^{13}C NMR** (101 MHz, Acetone) δ 198.0, 195.7, 190.8, 171.2, 165.7, 156.3, 153.8, 153.6, 145.8, 144.6, 142.7, 141.7, 127.5, 126.2, 125.9, 125.8, 124.8, 123.9, 122.4, 121.8, 121.4, 120.7, 110.8, 110.3, 79.2, 38.4, 14.2. Anal. calc. found: C 43.52; H 2.29; N 7.42; S 8.49%; molecular formula $[ReCl(CO)_3(N_4S_2C_{25}H_{18})]\cdot 1/3(CHCl_3)$ requires: C 43.40; H 2.36; N 7.15; S 8.18%. DSC: T_m = 316 °C (I heating scan); T_g = 206 °C (II heating scan) [32].

2.2.6. *[ReCl(CO)$_3$(4-(N-ethylcarbazol-3-yl)-2,6-di(pyrazin-2-yl)pyridine-κ^{2}N)], 6*

Yield: 52%. IR (KBr, cm^{-1}): 2021(vs), 1917(s) and 1892(vs) ν(C≡O); 1611(m) and 1591(s) ν(C=N) and ν(C=C). **^{1}H NMR** (400 MHz, DMSO) δ 10.44 (s, 1H), 9.45 (s, 1H), 9.19 (s, 2H), 9.15 (d, J = 2.2 Hz, 1H), 9.00 (d, J = 3.0 Hz, 1H), 8.95 (s, 2H), 8.57 (s, 1H), 8.43 (d, J = 8.7 Hz, 1H), 8.33 (d, J = 7.8 Hz, 1H), 7.87 (d, J = 8.7 Hz, 1H), 7.71 (d, J = 8.2 Hz, 1H), 7.55 (t, J = 7.6 Hz, 1H), 7.32 (t, J = 7.4 Hz, 1H), 4.56 (q, J = 7.0 Hz, 2H), 1.38 (t, J = 7.0 Hz, 3H). **^{13}C NMR** (125 MHz, DMSO) δ 197.1, 195.2, 190.2, 159.0, 155.7, 154.2, 152.2, 151.6, 148.2, 147.4, 146.3, 146.2, 145.8, 144.6, 141.8, 140.7, 127.1, 126.1, 124.9, 124.8, 123.6, 122.9, 121.3, 121.2, 120.2, 110.5, 110.3, 37.8, 14.3. Anal. calc. found: C 48.88; H 2.51; N 11.72%; molecular formula $[ReCl(CO)_3(N_6C_{27}H_{20})]$ requires: C 49.08; H 2.75; N 11.45%. DSC: T_m = 311 °C.

2.3. Crystal structure determination and refinement

X-ray diffraction data for complexes **2, 3** and **6** were collected at room temperature using Oxford Diffraction four-circle diffractometer Gemini An Ultra with Atlas CCD detector using graphite monochromated MoKα radiation (λ = 0.71073 Å). Diffraction data collection, cell refinement and data reduction were performed using the CrysAlis^{Pro} software [65]. The structures were solved by the direct methods using SHELXS and refined by full-matrix least-squares on F^2 using SHELXL-2014 [66,67]. All the non-hydrogen atoms were refined anisotropically, and hydrogen atoms were placed in calculated positions and refined with riding constrains: d(C–H) = 0.93 Å, U_{iso}(H) = 1.2 U_{eq}(C) (for aromatic) and d(C–H) = 0.96 Å, U_{iso}(H) = 1.5 U_{eq}(C) (for methyl). The methyl groups were allowed to rotate about their local threefold axis. Details of the crystallographic data collection, structural determination, and refinement for **2**, **3** and **6** are given in Table S1, ESI.

Crystallographic data for **2, 3** and **6** have been deposited with the Cambridge Crystallographic Data Center, CCDC 2042413–2042415. Copies of this information may be obtained free of charge from the Director, CCDC, 12 Union Road, Cambridge CB2 1EZ, UK (Fax: +44 1223 336033; e-mail: deposit@ccdc.cam.ac.uk or www.ccdc.cam.ac.uk).

2.4. Physical measurements

IR spectra were measured with a Nicolet iS5 FTIR spectrophotometer (4000–400 cm^{-1}) in the form of KBr pellets.

UV–Vis measurements were carried out using ThermoScientific Evolution 220 Spectrometer in solutions and Jasco V570 UV–Vis–NIR Spectrometer in films deposited on a glass substrate and as blends with PVK:PBD on a glass substrate. ^{1}H NMR and ^{13}C NMR spectra were collected in 295 K on Bruker Avance 400 NMR spectrometer in dimethyl sulfoxide-d^6 or acetone-d^6.

Electrochemical measurements were performed on Eco Chemie Autolab PGSTAT128n potentiostat (argon-saturated acetonitrile, c = 10^{-3} mol/L, 0.1 M Bu_4NPF_6 as an electrolyte). Platinum electrode (⌀2 mm), platinum coil and silver wire were used as working, auxiliary and reference electrodes. Cyclic voltammetry (CV) and differential pulse voltammetry (DPV) were recorded with scan rates 0.1 V/s and 0.01 V/s, respectively. All the results were calibrated on ferrocene (Fc) as internal standard.

Steady-state photoluminescence emission spectra were measured with FLS-980 fluorescence spectrophotometer in solid state and solution at room temperature and in an ethanol:methanol (4:1 v:v) rigid matrix at 77 K. 450 W Xe lamp and photomultiplier (Hamamatsu, R928P) were used as light source and detector, respectively. Photoluminescence spectra in solid state as film deposited on a glass substrate and as blends with PVK:PBD on a glass substrate were collected on Hitachi F-2500 spectrometer. The photoluminescence lifetimes were measured using time correlated single photon counting (TCSPC) or multi-channel

Table 3
The energies and characters of spin-allowed electronic transitions assigned to the lowest wavelength absorption bands of complexes **1**–**6**.

Complex	Experimental absorption λ_{exp} [nm] (10^4 ε [$M^{-1}cm^{-1}$])	Calculated transitions				
		Major contribution (%)	Character	E [eV]	λ [nm]	Oscillator strength
1	379 (1.0)	H → L (97%)	MLCT	2.78	445.72	*0.0113* S_1
		H-1→L (96%)	MLCT	2.98	415.66	*0.1401* S_2
		H-2→L (95%)	MLCT	3.26	380.77	*0.0058* S_3
2	397 (0.5)	H → L (97%)	MLCT	2.66	466.25	*0.0036* S_1
		H-1→L (96%)	MLCT	2.87	431.47	*0.1383* S_2
		H-2→L (92%)	MLCT	3.13	395.50	*0.0140* S_3
3	407 (0.6)	H → L (98%)	MLCT	2.59	478.05	*0.0138* S_1
		H-1→L (97%)	MLCT	2.82	439.41	*0.1157* S_2
		H-3→L (88%)	MLCT	3.08	402.62	*0.0052* S_3
4	389 (1.0)	H-1 → L (72%)	MLCT	2.87	431.94	*0.0642* S_1
		H → L (24%)	ILCT			
		H → L (60%)	ILCT	2.98	415.90	*0.3616* S_2
		H-1 → L (27%)	MLCT			
		H-2 → L (10%)	MLCT			
		H-2 → L (67%)	MLCT	3.19	389.10	*0.0128* S_3
		H-3 → L (17%)	ILCT			
		H → L (14%)	ILCT			
		H-4 → L (98%)	ILCT	3.38	367.25	*0.0022* S_4
		H-3 → L (74%)	ILCT	3.46	358.00	*0.0472* S_5
		H-2 → L (19%)	MLCT			
		H → L+1 (89%)	ILCT	3.56	348.33	*0.1657* S_6
5	406 (2.1)	H-1 → L (55%)	MLCT	2.80	442.44	*0.1053* S_1
		H → L (38%)	ILCT			
		H → L (51%),	ILCT	2.87	432.53	*0.2878* S_2
		H-1 → L (43%)	MLCT			
		H-3 → L (46%)	MLCT	3.08	402.39	*0.0054* S_3
		H-2 → L (42%)	ILCT/MLCT			
		H → L (10%)	ILCT			
		H-4 → L (85%)	ILCT	3.29	376.34	*0.0179* S_4
		H-2 → L (43%)	ILCT/MLCT	3.32	372.70	*0.0349* S_5
		H-3 → L (42%)	MLCT			
		H-4 → L (11%)	ILCT			
		H → L+1 (93%)	ILCT	3.37	367.47	*0.2248* S_6
6	413 (1.7)	H-1 → L (59%)	MLCT	2.61	475.71	*0.0857* S_1
		H → L (37%)	ILCT			
		H → L (54%)	ILCT	2.74	452.60	*0.2369* S_2
		H-1 → L (36%)	MLCT			
		H-3 → L (64%)	MLCT	2.95	420.72	*0.0149* S_3
		H-2 → L (26%)	ILCT			
		H-4 → L (97%)	ILCT	3.15	394.03	*0.0033* S_4
		H-2 → L (65%)	ILCT	3.19	389.08	*0.0184* S_5
		H-3 → L (29%)	MLCT			
		H → L+1 (91%)	ILCT	3.38	367.33	*0.2285* S_6

scaling (MCS) method, with additional measurement of the IRF for the analysis of a fluorescence decay. The quantum yields were determined using integrating sphere absolute method for argon bubbled solutions and solid states (powders). In each measurement, a solvent ($CHCl_3$ or CH_3CN) and Spectralon® were used as reference for diluted solutions and for powder samples, respectively. The emission correction file was applied to take into account the sensitivity of the monochromator, detector, sphere coating and optics to wavelength. Each scans were conducted with 0.25 nm step, 0.2 dwell time as well as repeated 3 times. The FLS-980 software was used to designate the quantum yield values.

A precise voltage supply (Gw Instek PSP-405) with the sample fixed to an XYZ stage was applied to collect electroluminescence (EL) spectra, and all the measurements were performed using procedure reported in our previous works [29–33], briefly described in ESI.

Differential Scanning Calorimetry (DSC) studies were carried out with the use of TA-DSC 2010 apparatus under nitrogen atmosphere, with heating rate 20 °C/min. Thickness of active layers was determined with atomic force microscopy (AFM) Topometrix Explorer TMX 2000.

Femtosecond transient absorption spectra were collected on Helios pump-probe transient absorption spectrometer (Ultrafast Systems) with the system setting as in Ref. [46], and briefly described in ESI. Samples of **1**, **4** and [$ReCl(CO)_3$(*terpy*-κ^2N)] were dissolved in chloroform to get the absorbance of 0.4–0.5 in the excitation wavelength (concentrations between $1.5 \times 10^{-4} - 5 \times 10^{-4}$ M). Solutions were placed in a 2 mm path length quartz cells with magnetic stirring and excited with 420 nm pump pulse (or additionally with 355 nm pump pulse in case of **1**). Obtained data was analyzed using Surface Xplorer (Ultrafast Systems) and Optimus™ [68] software. More details concerning the performed analyses were given in ESI.

2.5. Computational details

Theoretical calculations (singlet geometry optimization, molecular orbital analysis, absorption spectra, ionization potentials, electronic affinities, and reorganization energies) were performed using GAUSSIAN-09 program package [69] at the DFT or TD-DFT level with PBE1PBE hybrid exchange-correlation functional [70,71], and the basis sets were def2-TZVPD for rhenium and def2-TZVP for other elements [72–74]. The polarizable continuum model (PCM) correction was used to simulate the acetonitrile solvent environment for all calculations [75–77]. After optimization of the geometry, vibrational frequencies were calculated to verify the minimum on the potential energy surface.

3. Results and discussion

3.1. Synthesis and molecular structure

To synthesize 2,2′:6′,2″-terpyridine, 2,6-di(thiazol-2-yl)pyridine and

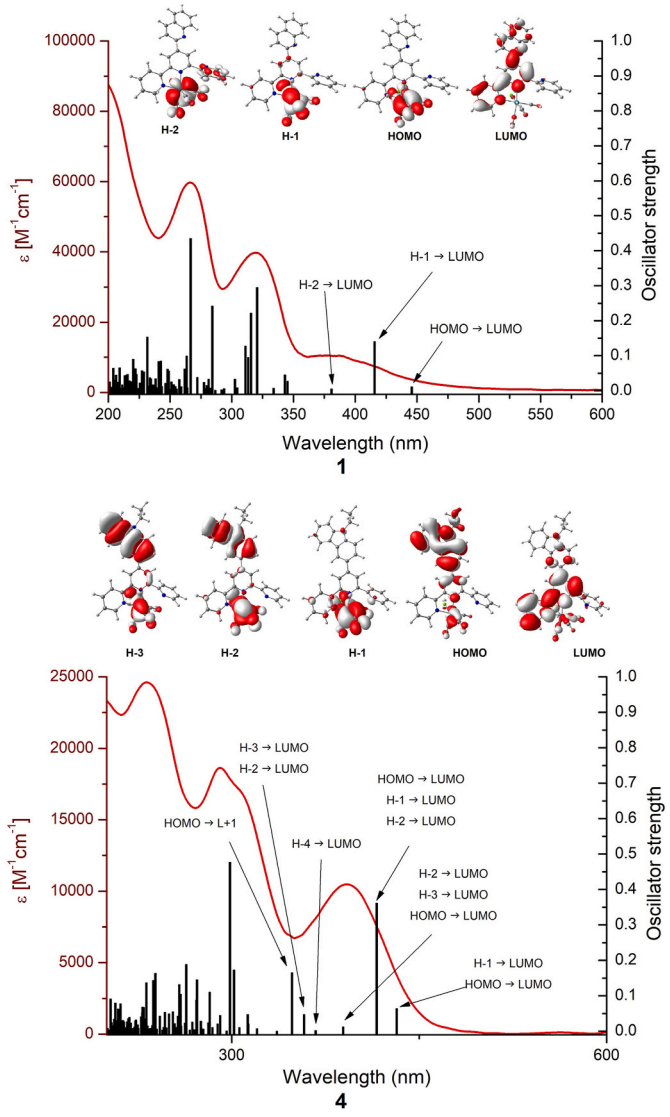

Fig. 3. Experimental (red line) absorption spectra of 1 and 4 in CH_3CN alongside with transitions (black) computed at TD-DFT/PCM/PBE0/def2-TZVPD/def2-TZVP level with the use of the PCM model at polarities corresponding to CH_3CN.

2,6-di(pyrazin-2-yl)pyridine functionalized with quinolin-2-yl and N-ethylcarbazol-3-yl pendant substituents (L^1–L^6), an efficient Kröhnke condensation was employed, while metalation of L^1–L^6 to the $Re(CO)_3^+$ core was performed by using standard procedure based on the reaction of $[Re(CO)_5Cl]$ with one equivalent of the corresponding ligand [29–33].

The obtained ligands L^1–L^6 and Re(I) complexes **1**–**6** provided satisfactory analytical data (Figs. S1–S3). Due to coordination of L^n in a bidendate way, two sets of signals for the peripheral rings of *terpy*/*dppy*/*dtpy* were observed in the ^1H NMR spectra of **1**–**6,** in contrast to the free ligands (Figs. S2–S3 in ESI). Facial geometry of the carbonyl groups in $[ReCl(CO)_3(L^n\text{-}\kappa^2N)]$ was indicated by the typical for this geometry set of $\nu(C{\equiv}O)$ absorptions, that is a sharp and intense high-energy absorption (2017–2027 cm^{-1}) and two overlapping lower-energy bands (1935–1882 cm^{-1}) (Fig. S1 in ESI). The average CO stretching frequencies (1937 cm^{-1} for **1**, 1946 cm^{-1} for **2**, 1959 cm^{-1} for **3**, 1938 cm^{-1} for **4**, 1942 cm^{-1} for **5**, 1943 cm^{-1} for **6**) indicate a decrease of the overall donor ability (including both σ-donor and π-acceptor contributions) of the chelating ligand upon replacing peripheral pyridine rings of *terpy* (**1** and **4**) by thiazole (**2** and **5**) and pyrazine ones (**3** and **6**) [78].

The molecular structures **2**, **3** and **6** were additionally confirmed by X-ray analysis. The crystallographic data, bond distances and angles, as well as intra- and intermolecular interactions in the crystal lattice are presented in ESI (Tables S1–S4 and Figs. S4–S6), while molecular structures of **2**, **3** and **6** together with the atom numbering are shown in Fig. 1.

In each complex, the Re(I) metal centre is coordinated to three facial carbonyl groups, as preliminarily suggested by the IR spectra analysis, two nitrogen atoms of L^n acting as a bidentate chelating ligand and chloride ion in *trans* position to the carbonyl ligand. Typically for complexes $[ReCl(CO)_3(L^n\text{-}\kappa^2N)]$, the bite angles N(2)–Re(1)–N(1) are noticeably smaller than an ideal value 90° for octahedron due to κ2N-coordination of the ligand L^n-κ^2N [74.7° for 2, 74.1° for 3, 75.1° for 6], contrary to C(1)–Re(1)–N(2) ones [102.5° for 2, 102.5° for 3, 102.2° for 6], which are enlarged as a result of noticeable steric interaction of the uncoordinated peripheral ring with the carbonyl ligand C(1)–O(1). Furthermore, the Re(1)–N(2) bond length to the central pyridine ring [2.253(3) Å for 2, 2.211(4) Å for 3, 2.216(3) Å for 6] is longer than Re(1)–N(1) distance to the peripheral ring [2.141(4) Å for 2, 2.161(4), Å for 3, 2.152(3) Å for 6]. The quinolin-2-yl plane in **2** is almost coplanar with the central pyridine ring of L^n (1.76°), while the substituent in **3** and **6** is slightly twisted away from the central pyridine ring of L^n (12.37° in **3** and 17.14° in **6**). The dihedral angles between the central pyridine and coordinated thiazole/pyrazine planes are 11.23°, 6.55° and 10.31° for **2**, **3** and **6**, while the uncoordinated peripheral ring is inclined to the central pyridine ring at 56.37°, 55.73° and 54.04°, respectively.

The synthesized Re(I) complexes exhibited high melting temperature (T_m) in the range of 294–327 °C detected by DSC measurements (cf. Experimental section). The replacement of quinolin-2-yl (**1**–**3**) with N-ethylcarbazol-3-yl group (**4**–**6**) increases T_m of the resulting Re(I) complexes. All complexes melted together with thermal decomposition, except for compounds based on *dtpy* (**2** and **5**). In the case of *dtpy* with attached quinoline (**2**) during first heating scan crystal-crystal transition at temperature between 171 and 190 °C, and crystallization exotherm at 206 °C, and next melting at 294 °C were observed. The second heating run of compounds with *dtpy* (**2** and **5**), after cooling, revealed only the glass transition (T_g) at 182 (**2**) and 206 °C (**5**) [32], which indicates formation of stable molecular glasses.

3.2. Electrochemistry

To estimate experimentally HOMO and LUMO energy levels, the compounds **1**–**6** were studied by cyclic voltammetry (CV) and differential pulse voltammetry (DPV). The CV and DPV methods give access to ionization potentials (IP) and electron affinities (EA), which are closely related to HOMO and LUMO energy levels. IP and EA energies were calculated using onsets of cathode and anode peaks, assuming that IP of ferrocene is −5.1 eV [79]. The electrochemical data of **1**–**6** are summarized in Tables 1 and S6, while their CV and DPV voltammograms are shown in ESI materials (Fig. S7).

For both series **1**–**3** and **4**–**6**, the first reduction potential shifted to more positive values in the order $[ReCl(CO)_3(4'\text{-R-}terpy\text{-}\kappa^2N)$ (**1**, **4**) < $[ReCl(CO)_3(4\text{-R-}dtpy\text{-}\kappa^2N)]$ (**2**, **5**) < $ReCl(CO)_3(4\text{-R-}dppy\text{-}\kappa^2N)]$ (**3**, **6**). On the other hand, the difference in the observed first reduction potential (E_{red}) between the complexes with different heteroaromatic groups attached to the central pyridine ring of L^n was in each case lower than 0.1 V. These findings allowed us to assign the first reduction wave to triimine-centred reduction process. Such an assignment is consistent with TD-DFT calculations showing stabilization of the ligand-centred LUMO orbital upon introduction of an additional S- or N-donor atom into the π-deficient trisheterocyclic unit of *dtpy* and *dppy*, respectively.

Also, the first oxidation potential (E_{ox}) was more affected by the triimine core than heteroaromatic group attached to the central pyridine. The Re(I) complexes with the 2,2′:6′,2″-terpyridine ligands (**1** and **4**) were found to be the easiest to oxidize, while those bearing with 2,6-

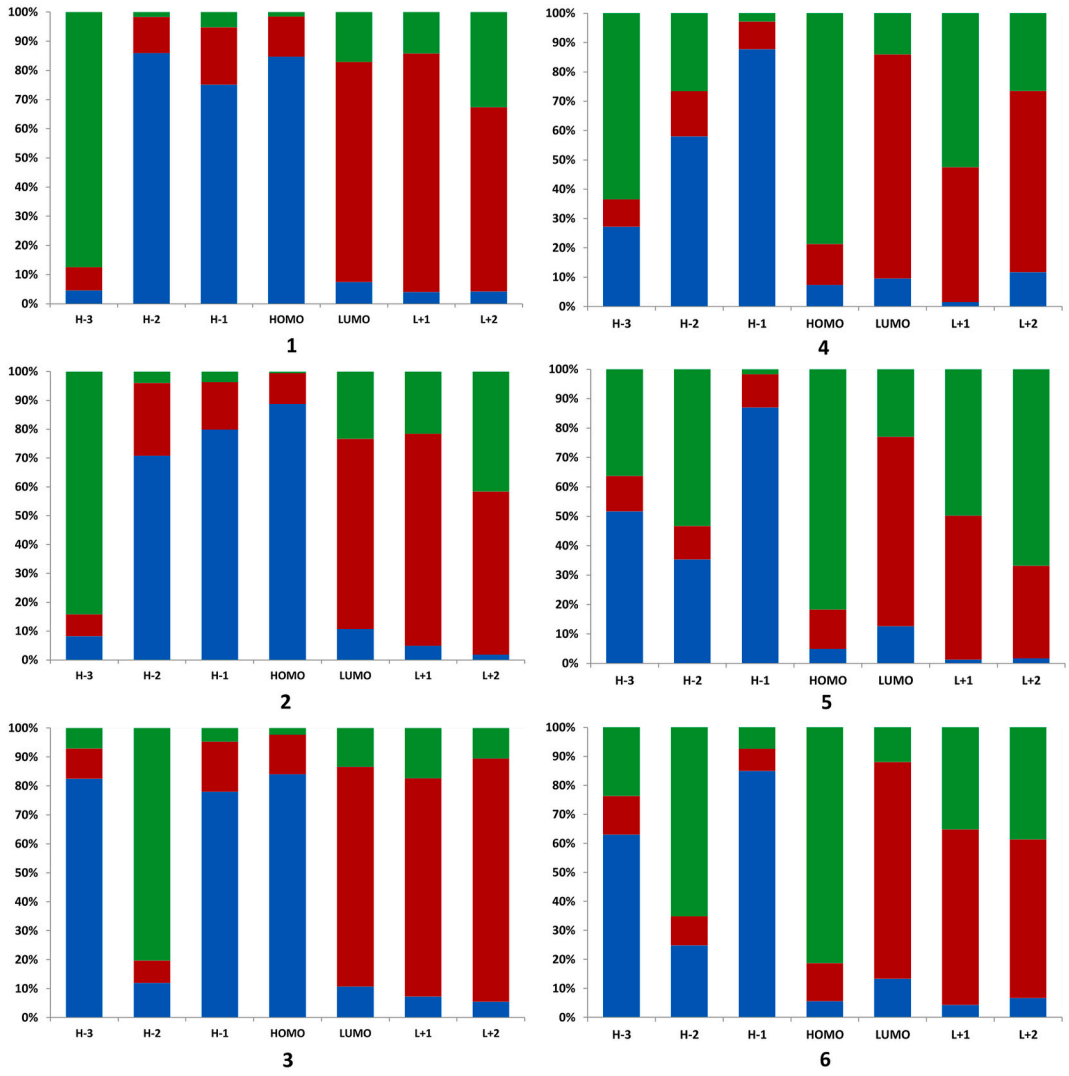

Fig. 4. Percentage composition of selected molecular orbitals calculated for complexes **1**–**6**. green – substituent R; red – triimine core (*terpy*, *dtpy* or *dppy*); blue – {$ReCl(CO)_3$} moiety.

Table 4
Summary of photoluminescent properties of complexes **1**–**6**.

	CH_3CN				$CHCl_3$				solid				CH_3OH:C_2H_5OH (77 K)			film	
	λ_{ex} [nm]	λ_{em} [nm]	τ_{av} [ns]	ϕ [%]	λ_{ex} [nm]	λ_{em} [nm]	τ_{av} [ns]	ϕ [%]	λ_{ex} [nm]	λ_{em} [nm]	τ_{av} [ns]	ϕ [%]	λ_{ex} [nm]	λ_{em} [nm]	τ_{av} [ns]	λ_{ex} [nm]	λ_{em} [nm]
1	390	663	2.7	<0.01	389	668	3.5	0.98	430	598	236.6	7.74	380	585, 548, 508	116 518.7	400	566
2	396	771	2.4	<0.01	413	754	4.1	1.01	496	648	3.1	4.16	400	608	1 518.9	415	581
3	406	736	3.2	<0.01	428	737	4.0	0.49	482	642	34.9	6.47	390	609	1 760.9	415	616
4	376	631	3.4	0.73	398	652	6.3	0.49	462	588	271.3	14.12	415	518, 551	36 928.7	420	550
5	403	711	5.7	0.79	418	712	8.5	1.23	490	635	85.1	3.50	420	548, 574	6 161.2	430	610
6	415	720	4.5	0.48	421	723	6.2	0.66	533	661	69.6	4.12	435	572	22 344.3	446	600

τ_{av} – average lifetime of multi-exponential fits of decay curves.
ϕ – luminescence quantum yield.

di(pyrazin-2-yl)pyridines (**3** and **6**) showed the highest values of E_{ox}. By analogy to the related [$ReCl(CO)_3(L^n\text{-}\kappa^2N)$] [80], it is highly probable that the first oxidation wave corresponds to Re(I)-based oxidation process Re(I)/Re(II).

Regarding the electrochemical gap, it can be noticed that E_g value was decreasing in the order [$ReCl(CO)_3$(4′-R-*terpy*-κ^2N) < [$ReCl(CO)_3$(4-R-*dtpy*-κ^2N)] < $ReCl(CO)_3$(4-R-*dppy*-κ^2N)] for both the series of **1**–**3** and **4**–**6**, while the replacement of quinolin-2-yl by N-ethylcarbazol-3-yl resulted in an increase of E_g (see Table 1).

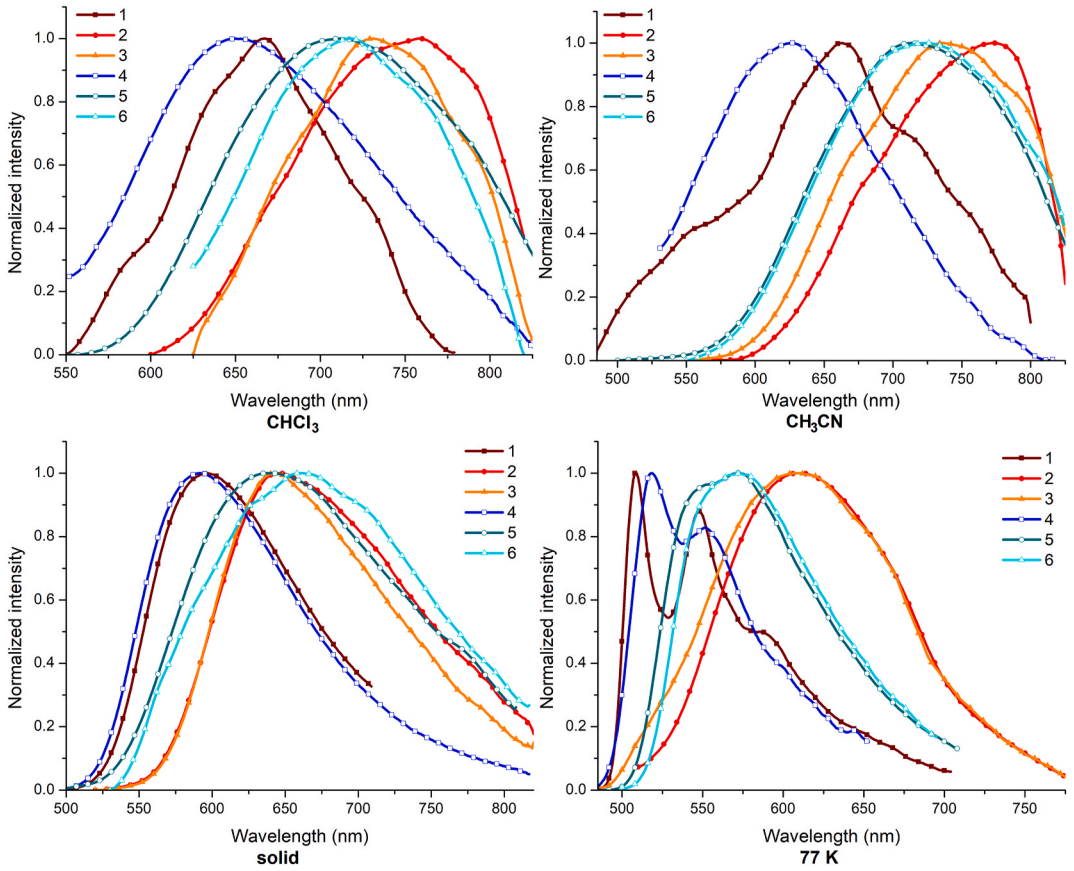

Fig. 5. Normalized emission spectra of **1**–**6** in non-polar and polar solvents ($CHCl_3$, ε = 4.8 and CH_3CN, ε = 37.5), solid state, and low temperature glass (77 K CH_3OH:C_2H_5OH 1:4 v:v).

3.3. UV-VIS absorption spectra

The UV–Vis spectra of **1**–**6** in solution and in film are shown in Figs. S8–S9, while their spectral parameters are summarized in Table 2. All complexes showed absorption characteristics of typical Re(I) carbonyl chromophores. They feature intense high-energy absorption bands corresponding to π→π* transitions localized on the organic ligand L^n and moderate absorption in the visible region of 350–500 nm, tentatively attributed to the metal-to-ligand charge-transfer (MLCT) electronic transitions, with possible contribution of intraligand charge-transfer (ILCT) electronic transitions in the case of **4**–**6** bearing electron-donating carbazole unit (Fig. 2).

For both series of **1**–**3** and **4**–**6**, by varying the triimine core, the absorption maximum of the charge-transfer band was bathochromically shifted in the order $[ReCl(CO)_3(4'\text{-R-}terpy\text{-}\kappa^2N)]$ (**1**, **4**) < $[ReCl(CO)_3(4\text{-R-}dtpy\text{-}\kappa^2N)]$ (**2**, **5**) < $ReCl(CO)_3(4\text{-R-}dppy\text{-}\kappa^2N)]$ (**3**, **6**), both in CH_3CN and $CHCl_3$. The appended heteroaromatic substituent had rather little effect on the energy of the lowest-energy absorption, but the replacement of quinolin-2-yl (**1**–**3**) by N-ethylcarbazol-3-yl (**4**–**6**) resulted in a significant increase in molar absorption coefficients of the long-wavelength absorption band for **4**–**6**, implying larger contribution of ligand-centred transitions in this band (Fig. 2). However, it should be noted that the lack of systematic changes in the energy of the lowest-energy absorption depending on the appended heteroaromatic group may be to some extent attributed to a relatively large experimental error in determining maxima of very broad absorption bands of **1**–**6**.

Upon going from non-polar chloroform to polar acetonitrile solution, the CT absorption of each Re(I) complex moved towards higher energy region, demonstrating negative solvatochromism frequently reported for Re(I) chromophores [29,30]. UV–Vis spectra of investigated Re(I) carbonyl complexes in film deposited on glass exhibited bands in similar absorption ranges to those observed in chloroform solution. However, in the case of film prepared from Re(I) complexes with electron-donating unit, the bathochromic shift of λ_{max} relative to solution was seen.

3.4. Theoretical insight into absorption spectroscopic properties of 1–6

The electronic transitions of **1**–**6** were also predicted by time-dependent density functional theory (TD-DFT). The calculated parameters of electronic transitions assigned to the low-energy absorption band of **1**–**6** are listed in Table 3, while the experimental absorption spectra of **1**–**6** alongside with the predicted electronic transitions are shown in Fig. 3 and Fig. S10.

According to the TD-DFT calculations, the low-energy absorption band of **1**–**3** is contributed by the electronic excitations from the HOMO, H-1 and H-2 or H-3 to LUMO. The highest oscillator strength involves the transition from the H-1 to LUMO (from 0.1157 for **3** to 0.1401 for **1**). The transitions HOMO→L and H-2/H-3→L with much lower oscillator strengths (from 0.0036 to 0.0140) fall at the red and blue edge of the visible absorption band, respectively (Table 3 and Fig. 3 and Figures S10). As the HOMO, H-1 and H-2 for **1**–**2** and HOMO, H-1 and H-3 for **3** spreads over the $\{Re(CO)_3Cl\}$ moiety and the LUMO resides on the triimine core, the electronic excitations in this region are of metal-to-ligand charge transfer (MLCT) character [81,82]. Small oscillator strengths of the MLCT transitions for **1**–**3** are reasoned by the poor overlap of the molecular orbitals involved in the electronic excitations.

On the contrary, the longest-wavelength absorption band of **4**–**6** is attributed to a combination of ^{1}MLCT and ^{1}ILCT transitions. The latter ones originate from charge delocalization from the carbazole unit to π-conjugated triimine acceptor moiety. The replacement of quinolin-2-yl by N-ethylcarbazol-3-yl in L^n results in changing the character of the highest occupied molecular orbital of the resulting Re(I) complexes **4**–**6**.

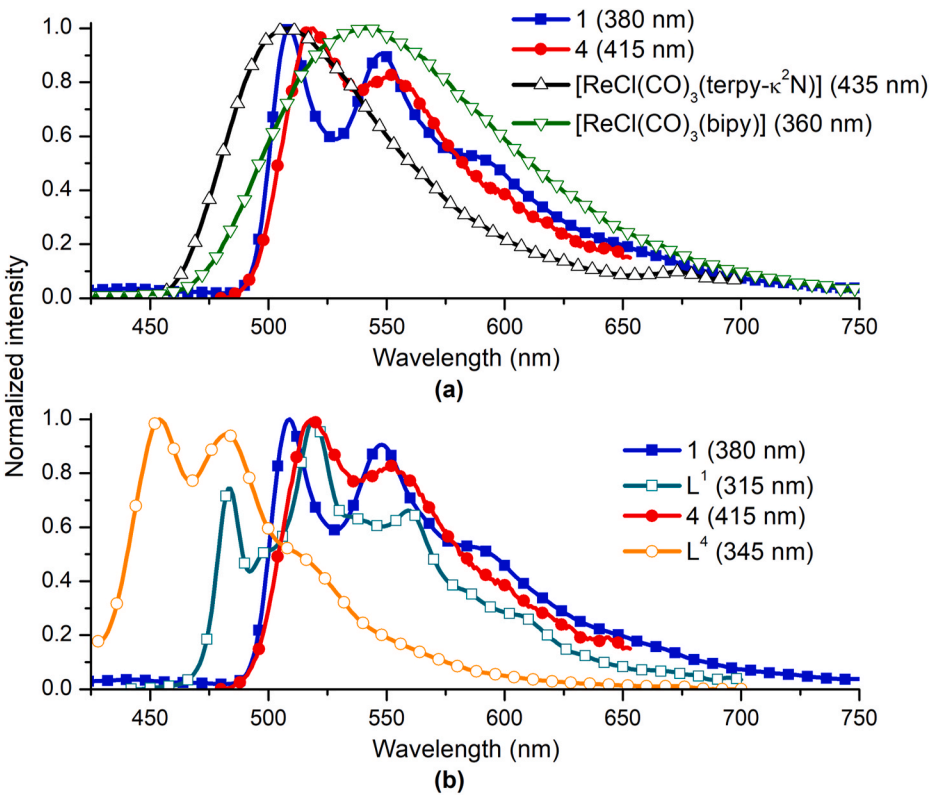

Fig. 6. Comparison of low temperature (77 K, EtOH:MeOH (4:1 v:v)) emission spectra of **1**, **4**, [ReCl(CO)$_3$(*terpy*-κ^{2}N)] and [ReCl(CO)$_3$(*bipy*)] (a); comparison of phosphorescence of **1**, L^1, **4** and L^4 (b). The triplet emission of L^4 was induced by addition of 10% ethyl iodide (EtI). The excitation wavelengths are given in parentheses.

As shown in Fig. 4, the HOMO of **4**–**6** resides predominately on electron-donating carbazole unit. A large contribution of N-ethylcarbazol-3-yl group is also theoretically indicated in H-3 for **4** and H-2 for **5** and **6**. In turn, the molecular orbitals H-1 and H-2 for **4** and H-1 and H-2 for **5** and **6** have significantly higher participation of 5d$_\pi$ rhenium, π^*_{CO} and π_{Cl} orbitals. In analogy to **1**–**3**, the LUMO of **4**–**5** is located on the triimine core. However, it should be noted that despite the change in the localization of the HOMO for complexes **4**–**6**, the $S_0 \rightarrow S_1$ electronic excitation conserves largely the MLCT character, which is rationalized by a predominant contribution of H-1→L in the $S_0 \rightarrow S_1$ excitation in these compounds (Table 3). The predominant MLCT character of the $S_0 \rightarrow S_1$ electronic excitation in **4**–**6** is also supported by the hypsochromic shift of the computed $S_0 \rightarrow S_1$ transition of **4**–**6** relative to $S_1 \rightarrow S_0$ for **1**–**3**. Due to the introduction of the electron-donating group, MLCT excited state is expected to be destabilized, which is manifested in the blue shift of the absorption band [83]. Larger percentage contribution of ^{1}ILCT transitions was found in the case of the $S_0 \rightarrow S_2$, $S_0 \rightarrow S_4$ and $S_0 \rightarrow S_6$ electronic excitations, also assigned to the longest-wavelength absorption band of **4**–**6**. Substantial increase in extinction coefficients of the lowest-energy absorption of **4**–**6** in comparison to **1**–**3** is reflected theoretically by higher oscillator strengths in the case of **4**–**6** due to contribution of intraligand charge-transfer (ILCT) transitions.

For both series of **1**–**3** and **4**–**6**, the experimentally observed bathochromic shift in an order [ReCl(CO)$_3$(4′-R-*terpy*-κ^{2}N)] < [ReCl(CO)$_3$(4-R-*dtpy*-κ^{2}N)] < [ReCl(CO)$_3$(4-R-*dppy*-κ^{2}N)] is nicely reproduced by TD-DFT calculations, and it correlates quite well with systematic lowering of the LUMO energy (Fig. S11).

3.5. Luminescence

The steady state photoluminescence (PL) and excitation spectra were recorded for **1**–**6** in non-polar and polar solvents ($CHCl_3$, $\varepsilon = 4.8$ and CH_3CN, $\varepsilon = 37.5$), solid state, low temperature glasses, and in the form of thin films on glass substrates (Table 4 and Figs. S12–S13 in ESI).

In solution at room temperature, all Re(I) compounds exhibited emission with maximum in the range 631–771 nm and very short lifetimes (2.4–8.5 ns). Low emission quantum yields of **1**–**6** (below 1.25%) demonstrate that the energy dissipates preferably via non-radiative pathways, as previously reported for many other polypyridinic Re(I) carbonyl complexes [29,30,32,83]. The broad and featureless photoluminescence emission bands of **1**–**6** at room temperature are indicative for MLCT nature of luminescence.

The MLCT origin of photoluminescence of **1**–**6** in solution at RT is also supported by the rigidochromic effect, manifested in the shifting of the emission band to higher energy relative to room temperature in the rigid solvent environment at 77 K or solid state (Fig. 5). Emissions arising from ^{3}CT states are very sensitive to the rigidity of the environment, contrary to ligand-localized triplet excited states ^{3}IL, essentially unperturbed by media conditions [84]. The excited-state lifetimes of **1**–**6** in the solid state and ethanol-methanol rigid-glass matrix at 77 K are significantly prolonged relative to those at room temperature, and the blue-shift upon going from solution to the solid state is accompanied with a significant increase of emission quantum yields. The largest emission efficiency in the solid state was found for **4**. Its quantum yield (14.12%) showed 2 to 4-fold enhancements in relation to the other studied complexes. Significant differences in the solid-state characteristics among these compounds and lack correlations with trends observed in dilute solutions seems to be attributed to packing variations of **1**–**6** due to inter- and intramolecular interactions between complex molecules. However, the phosphorescence emission upon aggregation (AIPE) effect cannot be excluded on the basis of the emission spectra of **1** and **4** in mixtures of acetonitrile and water (Fig. S14).

The frozen-state emission bands of **2**, **3**, **5** and **6** remain broad and non-structured, which indicates that the emission of these compounds at

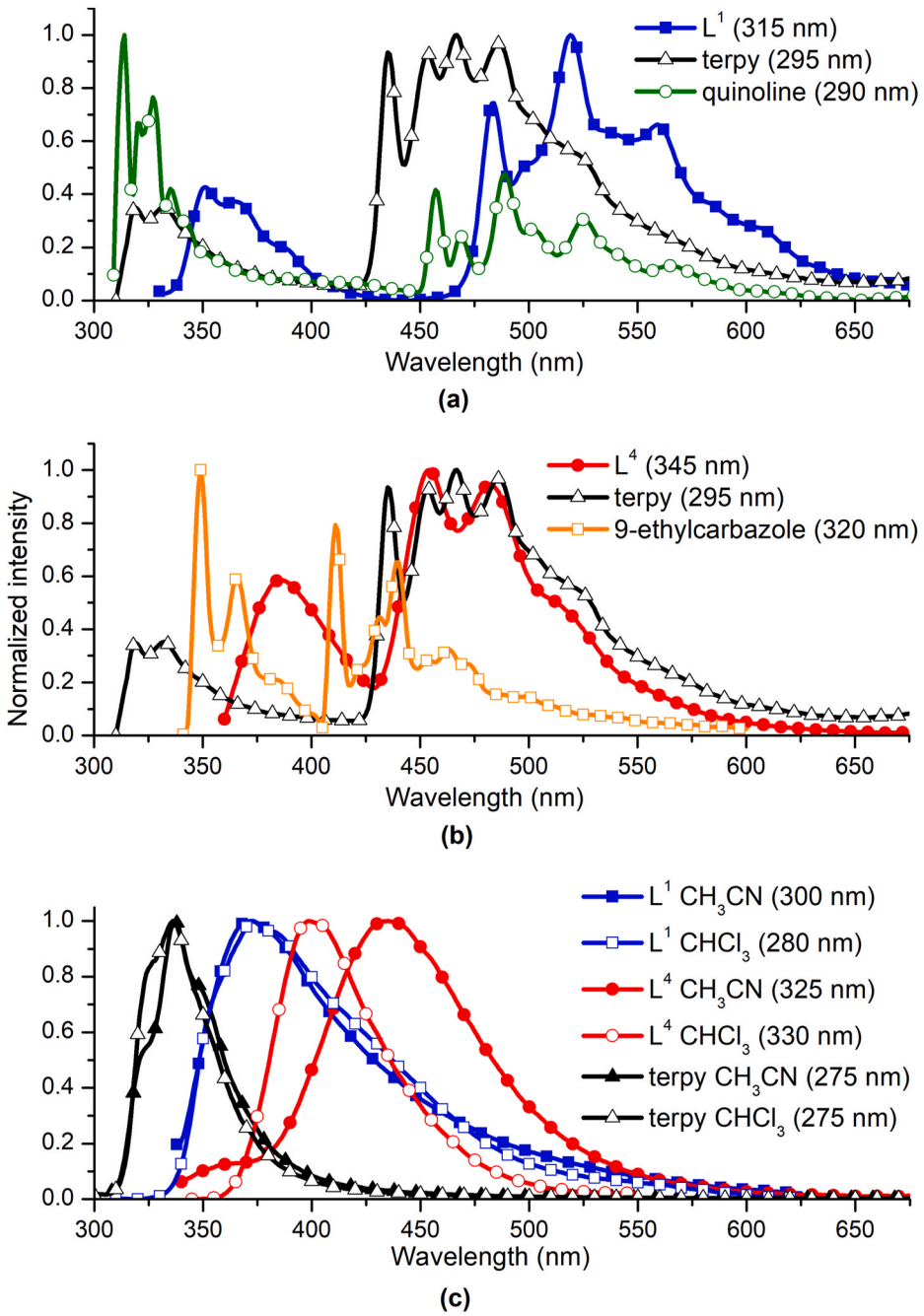

Fig. 7. 77 K emission of L^1 along with phosphorescence spectra of 2,2′:6′,2″-terpyridine and quinoline (a); 77 K emission of L^4 along with phosphorescence spectra of 2,2′:6′,2″-terpyridine and 9-ethylcarbazole (b); the RT emission of L^1, L^4 and 2,2′:6′,2″-terpyridine in different solvents (c). The triplet emission of L^4 and 9-ethylcarbazole was induced by addition of 10% ethyl iodide (EtI). The excitation wavelengths are given in parentheses.

77 K is still from ^{3}MLCT excited state. On the contrary, the emission profiles of **1** and **4** undergo substantial changes upon cooling to 77 K, and a high degree of vibronic structure becomes evident, signalling ^{3}IL or mixed ^{3}MLCT/^{3}IL character of the excited state. To get a better insight into the nature of frozen-state emission of **1** and **4**, the phosphorescence of the free ligands L^1 and L^4, and the emission of the parent complex [ReCl(CO)$_3$(*terpy*-κ^{2}N)] and strongly related [ReCl(CO)$_3$(*bipy*)] were recorded at 77 K in EtOH:MeOH rigid matrix. As shown in Fig. 6a, the 77 K emission band of [ReCl(CO)$_3$(*terpy*-κ^{2}N)] is non-structured, indicating that phosphorescence of these systems is from ^{3}MLCT excited state. It occurs in almost the same energy region as for examined Re(I) complexes with substituted *terpy*-ligands, and it is slightly blue-shifted compared to [ReCl(CO)$_3$(*bipy*)]. On the other hand, the phosphorescence spectrum of **1** at 77 K is largely coincident with the ^{3}IL phosphorescence measured for L^1, while the frozen-state emission of **4** appears at lower energy relative to phosphorescence measured for L^4 (Fig. 6b). Taking all these considerations, the 77 K emissions of **1** and **4** can be assigned to the phosphorescence from the excited state of mixed ^{3}MLCT/^{3}IL character. However, the contribution of ^{3}IL seems to be significantly larger in the case of **1**, which is also manifested in a noticeable increase of emission lifetime of **1** in relation to **4** (Table 4). The ^{3}IL excited states were estimated as 0.346 eV for **4** and 0.380 eV for **1**, supporting a larger energy gap between ^{3}MLCT and ^{3}IL in the case of **4** (Fig. S15).

Noteworthy, the phosphorescence of L^4 has significantly higher energy than L^1. By comparing the emissions of the free ligands (L^4 and L^1)

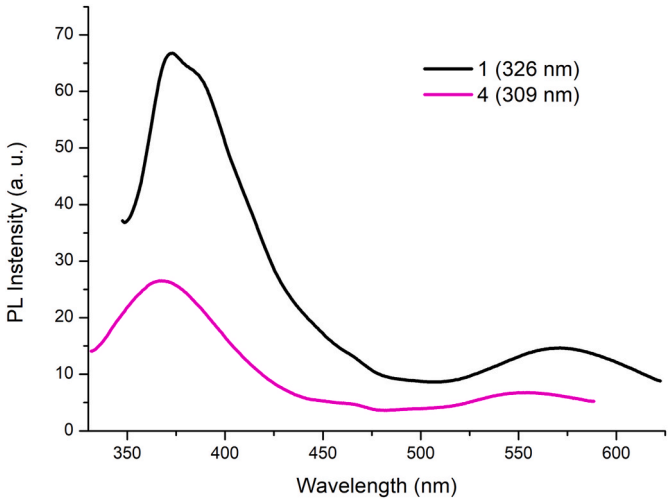

Fig. 8. Photoluminescence spectra of **1** and **4** in film. The excitation wavelengths are given in parentheses.

with reference molecules *terpy*, quinoline and N-ethylcarbazole (Fig. 7a and b) we can assume that the emitting triplet states of L^1 and L^4 is localized on different molecule units – 2,2′:6′,2″-terpyridine for L^4 and quinoline in the case of L^1. The ^{3}ILCT excited states in L^4 are inaccessible in agreement with the rigidochromic effect. Remarkably, also the fluorescence of L^4 at 77 K is not contributed by ^{1}ILCT. As shown in Fig. 7c, the 77 K fluorescence band of L^4 falls in the range of its RT emission in non-polar chloroform solution and it is blue shifted relative to that in acetonitrile at RT.

Photoluminescence spectra of Re(I) carbonyl complexes as film excited with λ_{ex} below 350 nm, that is, from the range of ligand transition, showed two emission bands: a more intense located around 400 nm and the second one above 500 nm (Fig. 8 and Fig. S16). Films excited with the wavelength from MLCT and ILCT electronic transitions exhibited weak emission with λ_{em} ranging from 500 to 616 nm.

Considering the effect of the triimine skeleton and appended heteroaromatic group, the designed complexes **1**–**6** show significant environment dependent emission. In both rigid media and solutions, the emission of [ReCl(CO)$_3$(4-R-*dtpy*-κ^{2}N)] (**2**, **5**) and [ReCl(CO)$_3$(4-R-*dppy*-κ^{2}N)] (**3**, **6**) is significantly red-shifted in relation to the emission of [ReCl(CO)$_3$(4′-R-*terpy*-κ^{2}N)] (**1**, **4**). In the case of films, the same tendency was found for the low energy emission band.

In solutions at room temperature, the emission maximum systematically moves toward longer wavelengths in the order [ReCl(CO)$_3$(4′-R-*terpy*-κ^{2}N)] (**1**) < [ReCl(CO)$_3$(4-R-*dppy*-κ^{2}N)] (**3**) < [ReCl(CO)$_3$(4-R-*dtpy*-κ^{2}N)] (**2**) for the series of complexes with quinolin-2-yl pendant substituent, while the emission of **5** and **6** covers almost the same range and displays a clear bathochromic shift relative to **4**. For all the pairs **1** and **4**, **2** and **5**, **3** and **6**, the emission of the Re(I) complexes with appended N-ethylcarbazol-3-yl group is hypsochromically shifted, in both CH_3CN and $CHCl_3$. The hypsochromic shift of the emission due to the introduction of electron-rich group can indicate that photophysical properties of the designed complexes are predominately controlled by the MLCT excited state. Attachment of the electron donating group to MLCT core is expected to destabilize the MLCT excited state [85]. The assignment of the lowest excited state in the designed complexes to MLCT character is also supported by the fact that excited-state lifetime of **1** and **4** quantitatively matches that of [ReCl(CO)$_3$(*terpy*-κ^{2}N)] [86].

Additionally, the capacity of the synthesized Re(I) carbonyl complexes for emission of light under voltage was examined in diodes with architecture ITO/PEDOT:PSS/complex/Al and ITO/PEDOT:PSS/PVK:PBD:complex/Al. In a guest-host type of device, the active layer consists of [ReCl(CO)$_3$(L^n-κ^{2}N)] dispersed (1, 2 and 15 wt%) in a mixture of poly (N-vinylcarbazole) (PVK) (50 wt %): 2-(4-tert-butylphenyl)-5-(4-biphenylyl)-1,3,4-oxadiazole (PBD) (50 wt %). Considering the electronic absorption range of the complexes and photoluminescence of PVK:PBD, the energy transfer from host to luminophore molecules due to Förster mechanism can be expected (Fig. 2c). This type of energy transfer can effectively occur if the PL spectrum of the host overlaps with the absorption spectrum of the guest. Considering the PL spectrum of applied

Table 5
Position of λ_{EL} of light emitted by diodes with structure ITO/PEDOT:PSS/PVK:PBD:complex/Al and its maximal measured emission intensity.

Complex	complex content in PVK:PBD matrix					
	1 wt%		2 wt%		15 wt%	
	λ_{EL} [nm]	Intensity	λ_{EL} [nm]	Intensity	λ_{EL} [nm]	Intensity
1	610	2121	610	1563	610	9513
2	640	955	640	931	640	1701
3	635	3054	630	871	640	49 445
4	590	32 799	580	194 520	588	26 831
5[a]	–	–	619	50 000	621	60 000
6	620	1521	615	19 395	615	25 598

– not investigated.
[a] data for complex **5** taken from Ref. [32].

Table 6
Summary of time components obtained from Global Lifetime Analysis (GLA).

Complex	Time constants, t_i [ps]				
	t_1	t_2	t_3	t_4	t_5
1	0.18	4.57	185.5	1290	–
	0.41[a]	41.57[a]	824.8[a]	–	–
	0.18[b]	4.86[b]	116.6[b]	885.2[b]	8332[b]
4	0.66	6.81	191.2	6180	–
[ReCl(CO)$_3$(*terpy*-κ^{2}N)]	0.62	5.97	26.74	3213	–
[ReCl(CO)$_3$(*bipy*)][c]	0.097[d]	3.3	16	inf	–

[a] t′ values taken from global analysis in 355–405 nm range.
[b] t values taken from global analysis of fsTA spectra after pumping at 355 nm.
[c] data taken from Refs. [87,88].
[d] data taken from fluorescence up-conversion from Refs. [87,88].

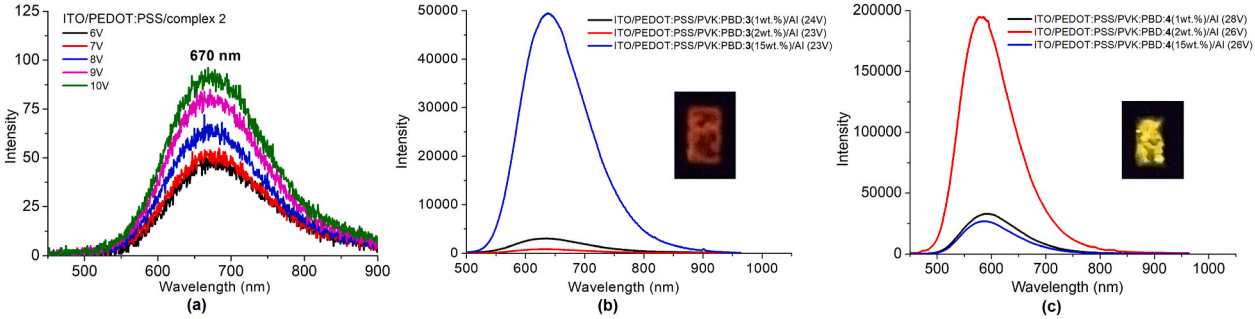

Fig. 9. Electroluminescence spectra and photos of selected diodes containing investigated Re(I) carbonyl complexes (see also Figs. S16–S17).

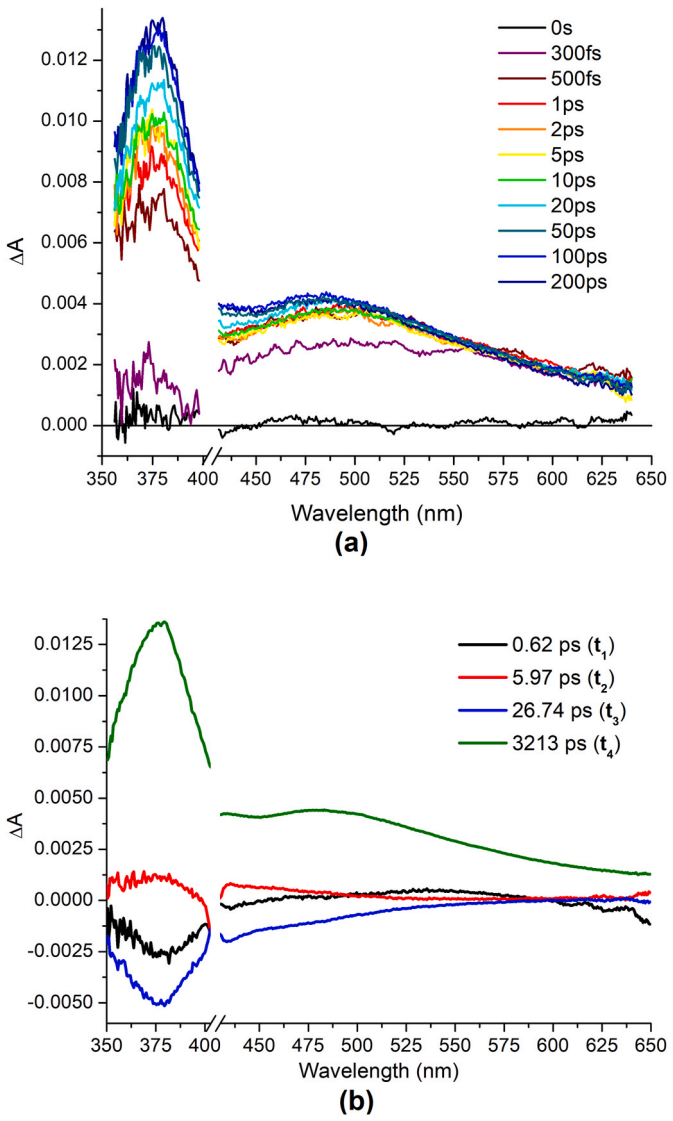

Fig. 10. (a) fsTA spectra of [ReCl(CO)$_3$(*terpy*-κ^{2}N)] in $CHCl_3$ solution (λ_{pump} = 420 nm, 0.21 μJ per pulse); (b) Decay Associated Spectra (DAS) for [ReCl(CO)$_3$(*terpy*-κ^{2}N)].

matrix and UV–vis spectra of Re(I) carbonyl complexes presented in Fig. 2c, it can be seen that only absorption band originated from MLCT and ILCT electronic transitions of the guest overlaps with the emission spectrum of the host. It was found that the devices with a neat complex applied as active layer contrary to diodes with guest-host configuration, were non emissive, except for the diode based on compound with *dtpy* skeleton with attached quinoline derivative (**2**) (Fig. 9a). As can be seen from Fig. 9a, this diode exhibited the maximum of emission band (λ_{EL}) at 670 nm corresponding to red light. Together with increase of Re(I) carbonyl complex content in a blend from 1 to 15 wt%, more intense light emission was seen (Fig. 9 and Table 5) with the exception of **4**. The fabricated diodes emitted light with maximum of electroluminescence band (λ_{EL}) ranging from 590 to 640 nm, which corresponds to emission of yellow and orange light (cf. Fig. 9c and b). The λ_{EL} position of device containing complexes consisted of *terpy* with attached carbazole (**4**) and quinoline (**1**) derivatives was blue-shifted compared to others. The most intense emission of light under external voltage exhibited diodes based on compounds with *terpy* (**4**) and *dtpy* skeleton (**5** [32]) substituted with carbazole unit. However, it can be noticed that the emission with the highest intensity was reached under high external voltage above 20 V.

3.6. Femtosecond transient absorption

To obtain a more complete picture of excited state processes in [ReCl(CO)$_3$(L^n-κ^{2}N)], transient absorption spectra in the femtosecond time-scale (fsTA) were recorded for chloroform solution of **1**, **4**, and a model complex [ReCl(CO)$_3$(*terpy*-κ^{2}N)] after excitation at 420 nm within the range 355–650 nm (Figs. 10 and 11, Figures. S18–S23). For **1**, for which PL studies revealed greater contribution of ^{3}IL, also the TA experiment with 355 nm pumping wavelength, allowing to excite both rhenium(I) carbonyl (MLCT) and organic ligand chromophores (IL), was undertaken. The data in the first 300 fs, which were strongly affected by cross-phase modulation and scattered pump light and could lead to unreliable conclusions, were not considered in the discussion. In the global lifetime analysis of the data obtained after excitation at 420 nm, the wavelength region (405–425 nm) was excluded as it covers scattered pump light.

The fsTA spectra of the parent complex [ReCl(CO)$_3$(*terpy*-κ^{2}N)] show two positive bands due to excited-state absorption (ESA), with maxima at 376 and 485 nm. On the basis of transient absorption studies of bipyridine (*bipy*) rhenium(I) analogue [ReCl(CO)$_3$(*bipy*)], which showed ESAs at 373 and ~480 nm, the band of [ReCl(CO)$_3$(*terpy*-κ^{2}N)] in the UV region can be assigned to the absorption of bipyridine anion radical *bipy*$^{\bullet-}$, while ESA in the visible part corresponds to Cl/L$^{\bullet-}$→Re (Ligand-to-Metal-Charge-Transfer, LMCT) transitions. The intense band at ~370 nm is regarded as diagnostic of *bipy* reduction upon excitation [87,88]. In view of the close resemblance of [ReCl(CO)$_3$(*terpy*-κ^{2}N)] to [ReCl(CO)$_3$(*bipy*)], we can assume that optically populated ^{1}MLCT state of [ReCl(CO)$_3$(*terpy*-κ^{2}N)] undergoes femtosecond intersystem crossing (ISC) into intermediate diimine-localized π→π* intraligand state (^{3}IL) and vibrationally hot ^{3}MLCT state of {ReCl(CO)$_3$}→*terpy*-κ^{2}N transition. The conversion from ^{3}IL to ^{3}MLCT occurs on a picosecond time scale, and the relaxed ^{3}MLCT state decays by minor radiative and major non-radiative pathways to the ground state [87,88].

The global lifetime analysis (GLA) confirmed that the TA data of [ReCl(CO)$_3$(*terpy*-κ^{2}N)] are the best described in terms of four components, each characterized by a time constant t_i (Fig. 10b). Likewise as for [ReCl(CO)$_3$(*bipy*)], the t_1, t_2, t_3 and t_4 can be assigned to the intersystem crossing from initially populated singlet state to the triplet manifold, conversion of the intermediate state ^{3}IL to the ^{3}MLCT, vibrational relaxation of the lowest triplet state ^{3}CT and ground state recovery time, respectively.

The close resemblance of the time t_4 (3213 ps) for DAS_4 in TA of [ReCl(CO)$_3$(*terpy*-κ^{2}N)] and the emission decay (τ = 3.0 ns in $CHCl_3$) [86] is suggestive that the emitting excited state can be attributed to observed in TA the lowest triplet state of ^{3}MLCT character, with small amount of π→π* *terpy*. Noteworthy, short ^{3}MLCT lifetimes in Re(I) complexes are rather rare, but not unprecedented. Exemplarily, for related rhenium(I) κ^{2}N-tricarbonyl complexes with 4′-(4-substituted-phenyl)-terpyridine ligands, short ^{3}MLCT lifetimes (from 0.58 to 2.3 ns) were confirmed using transient IR (TRIR) spectroscopy [83].

A remarkable shortening of the emitting triplet-state lifetime (τ = 3.0 ns in $CHCl_3$) of [ReCl(CO)$_3$(*terpy*-κ^{2}N)] relative to [ReCl(CO)$_3$(*bipy*)] (τ = 51.0 ns in $CHCl_3$) [86] can be largely assigned to the presence of dangling (non-coordinated) pyridine ring in [ReCl(CO)$_3$(*terpy*-κ^{2}N)], which results in a greater complex flexibility.

Regarding other Decay Associated Spectra (DAS) (see Table 6, Figs. 10 and 11 and Figures S18–S23), the difference between [ReCl(CO)$_3$(*terpy*-κ^{2}N)] and [ReCl(CO)$_3$(*bipy*)] concerns also t_1 and t_3 values associated with intersystem crossing and vibrational relaxation due to reorganization within a supramolecular cluster consisting of the Re(I) chromophore and local solvent molecules, respectively [88]. For [ReCl(CO)$_3$(*terpy*-κ^{2}N)], both these processes were determined to occur slower than in the case of [ReCl(CO)$_3$(*bipy*)] (see Table 6). Due to the rejection of the data affected by cross-phase modulation and scattered pump light, however, the accurate determination of ISC in [ReCl(CO)$_3$(*terpy*-κ^{2}N)] requires further studies with femtosecond fluorescence up-conversion methodology and/or TRIR spectroscopy, as it was

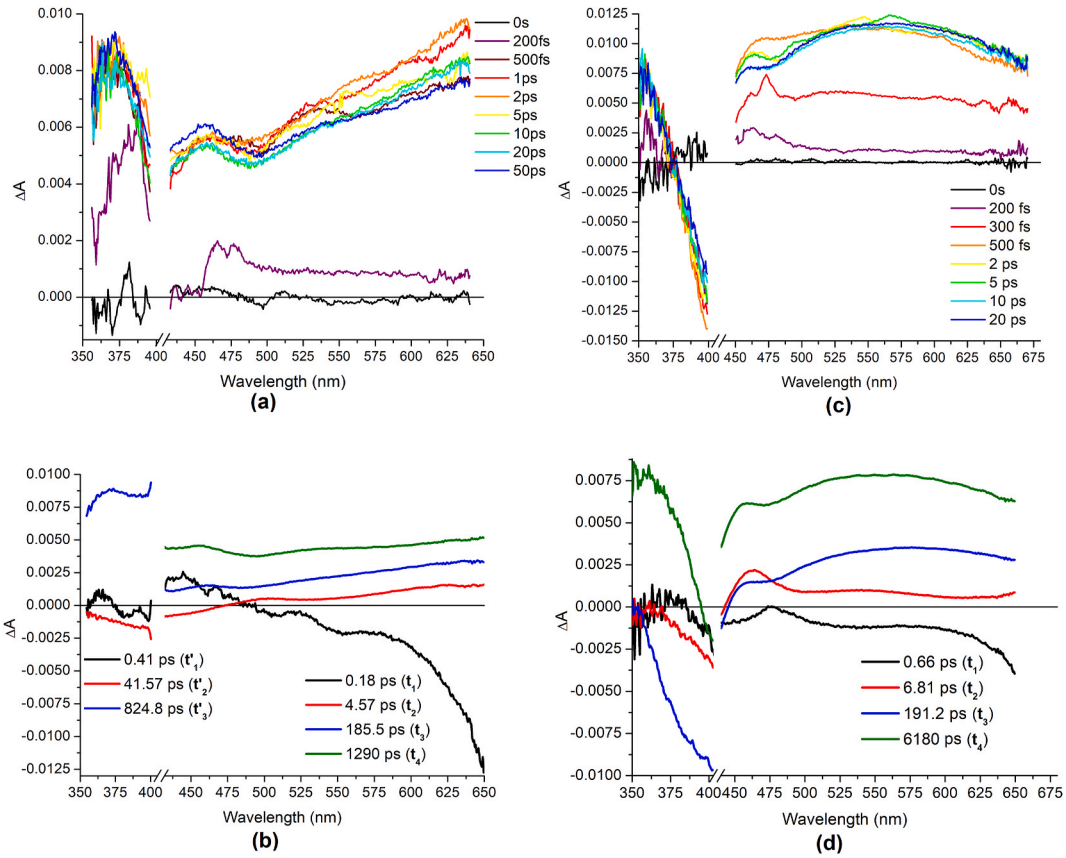

Fig. 11. fsTA and DAS spectra of compounds **1** (a–b) and **4** (c–d) in chloroform solutions (λ_{pump} = 420 nm, 0.21 μJ per pulse).

done for [ReCl(CO)$_3$(*bipy*)] [88].

Compared to [ReCl(CO)$_3$(*terpy*-κ^{2}N)], fsTA spectra of **1** and **4** display significantly broader absorption in the visible region, which can be attributed to extension of π-conjugation due to introduction of heteroaromatic group into *terpy* ligand (quinolin-2-yl in **1** and N-ethylcarbazol-3-yl in **4**). Differences in position of ESA assigned to the characteristic absorption of *bipy*$^{\bullet-}$ between **1** and **4** in comparison to the model complex [ReCl(CO)$_3$(*terpy*-κ^{2}N)] can be attributed to different electron-donating ability of appended heteroaromatic group. Due to introduction of the stronger electron-donating N-ethylcarbazol-3-yl group into *terpy* core, UV transition absorption of **4** is significantly blue-shifted in relation to [ReCl(CO)$_3$(*terpy*-κ^{2}N)], contrary to UV transition absorption of **1**, which falls in the same range as for the model complex.

Some differences between **1** and **4** can be also noticed as far as the global lifetime analysis is regarded. Similar to [ReCl(CO)$_3$(*terpy*-κ^{2}N)], the TA data of **4** were assigned to four components. On the contrary, the ESA bands of **1** in UV and Vis were found to possess different decay kinetics. In the spectral region 425–625 nm, the best fit to the experimental data after excitation at 420 nm was achieved with four components model (as in the case of **4**), while three compartments were used to describe the data in the range from 355 nm to 405 nm. These findings can be assigned to larger contribution of the ^{3}IL state, predominately participated in the UV region. The given explanation is supported also by the TA results obtained after excitation at 355 nm, allowing to excite both rhenium(I) carbonyl and organic ligand chromophores. In this case, the best fit to the experimental in the whole range (both UV and Vis) was achieved with the use of five components model, with time constants correlated to those determined in GLA with 420 nm pumping wavelength for UV and Vis regions (Table 6).

The values of t_4 for **1** and **4** (1290 ps for **1** and 6180 ps for **4**, see Table 6) match to the emission decays (1.4 ns for **1** and 6.3 ns for **4**), suggesting that the origin of these transient absorptions can be attributed to the emissive excited species. In comparison to the model complex [ReCl(CO)$_3$(*terpy*-κ^{2}N)], t_4 value slightly decreases in the case of **1**, while introduction of N-ethylcarbazol-3-yl group into *terpy* (**4**) leads to the small increase of t_4 (Fig. 11). However, negligible changes in the t_4 of **1** and **4** relative to [ReCl(CO)$_3$(*terpy*-κ^{2}N)] allow us to assign the lowest triplet state as ^{3}MLCT with π→π* 4′-R-*terpy* admixture as well as to exclude the thermal equilibrium between ^{3}CT and ^{3}IL responsible for reservoir effect [89]. The lowest triplet state in **1** and **4** has ^{3}MLCT character.

4. Conclusions

In this study, six rhenium(I) complexes bearing 2,2′:6′,2″-terpyridine (*terpy*), 2,6-di(thiazol-2-yl)pyridine (*dtpy*) and 2,6-di(pyrazin-2-yl)pyridine (*dppy*) with appended quinolin-2-yl and N-ethylcarbazol-3-yl groups were prepared, and the impact of the trisheterocyclic core (*terpy*, *dtpy* and *dppy*) and heterocyclic substituent on photophysical properties of obtained [ReCl(CO)$_3$(L^n-κ^{2}N)] was investigated with electrochemistry, absorption and emission spectroscopy, as well as theoretically using DFT calculations at the PBE1PBE/DEF2–TZVPD/DEF2-TZVP level. The introduction of an additional S- or N-donor atom into the π-deficient trisheterocyclic unit of *dtpy* and *dppy* resulted in the stabilization of the ligand-centred LUMO orbital, manifested experimentally in a significant red-shift of the absorption and emission of [ReCl(CO)$_3$(4-R-*dtpy*-κ^{2}N)] (**2**, **5**) and [ReCl(CO)$_3$(4-R-*dppy*-κ^{2}N)] (**3**, **6**) in relation to [ReCl(CO)$_3$(4′-R-*terpy*-κ^{2}N)] (**1**, **4**). The attachment of electron-donating N-ethylcarbazol-3-yl group into the triimine acceptor core gave rise to intraligand charge-transfer (ILCT) transitions from donor orbital localized on the substituent to triimine-based π*acceptor orbitals. The long-wavelength absorptions of **4**–**6** were assigned to a combination of ^{1}MLCT and ^{1}ILCT transitions. The contribution of ^{1}ILCT was reflected in the significant increase in molar absorption coefficients of the long-

wavelength absorptions of **4**–**6** compared to **1**–**3**. On the contrary, the lowest triplet state of all Re(I) compounds was found to have ^{3}MLCT character, with small admixture of π→π* in 4′-R-*terpy*. With reference to [ReCl(CO)$_3$(*bipy*)] and [ReCl(CO)$_3$(*terpy*-κ^{2}N)], it was evidenced that optically populated ^{1}MLCT state of **1** and **4** undergoes femtosecond intersystem crossing (ISC) into intermediate diimine-localized π→π* intraligand state (^{3}IL) and vibrationally hot ^{3}CT state of {ReCl(CO)$_3$}→*terpy*-κ^{2}N transition. The relaxed ^{3}MLCT state decays by major non-radiative and minor radiative pathways to the ground state. Negligible changes in the t_4 of ground state recovery time for **1** and **4** relative to [ReCl(CO)$_3$(*terpy*-κ^{2}N)] allowed us to exclude the thermal equilibrium between ^{3}CT and ^{3}IL responsible for reservoir effect. The findings of preliminary investigations of Re(I) complexes electroluminescence ability showed that the presence of *terpy* and carbazole units (**4**) resulted in emission of yellow light contrary to the diodes based on other compounds. The replacement of carbazole (**4**–**6**) with quinoline (**1**–**3**) structure bathochromically shifted the λ_{EL}. The most intense emission induced by external voltage was found for the devices with *terpy* (**4**) and *dtpy* (**5**) skeleton substituted with carbazole derivative.

CRediT authorship contribution statement

Katarzyna Choroba: Conceptualization, Methodology, Formal analysis, Investigation, Data curation, Visualization. **Sonia Kotowicz:** Investigation. **Anna Maroń:** Methodology, Formal analysis, Investigation, Visualization. **Anna Świtlicka:** Investigation. **Agata Szłapa-Kula:** Investigation. **Mariola Siwy:** Investigation, Visualization. **Justyna Grzelak:** Investigation. **Karolina Sulowska:** Investigation. **Sebastian Maćkowski:** Resources, Writing – review & editing, Funding acquisition. **Ewa Schab-Balcerzak:** Validation, Formal analysis, Resources, Writing – original draft, Writing – review & editing, Supervision. **Barbara Machura:** Conceptualization, Validation, Writing – original draft, Writing – review & editing, Supervision, Project administration, Funding acquisition.

Declaration of competing interest

The authors declare that they have no known competing financial interests or personal relationships that could have appeared to influence the work reported in this paper.

Acknowledgements

The work was supported by the National Science Centre of Poland grants no. 2017/25/B/ST5/01611 (BM) and 2017/27/B/ST3/02457 (JG and SM). The calculations were carried out in Wroclaw Centre for Networking and Supercomputing (http://www.wcss.wroc.pl).

Appendix A. Supplementary data

Supplementary data to this article can be found online at https://doi.org/10.1016/j.dyepig.2021.109472.

References

[1] Winter A, Newkome GR, Schubert US. Catalytic applications of terpyridines and their transition metal complexes. ChemCatChem 2011;3:1384–406. https://doi.org/10.1002/cctc.201100118.
[2] Zhang G, Liu E, Yang C, Li L, Golen JA, Rheingold AL. Copper(II) complexes of 2,2′:6′,2″-terpyridine derivatives for catalytic aerobic alcohol oxidations – observation of mixed-valence CuICuII assembles. Eur J Inorg Chem 2015;2015:939–47. https://doi.org/10.1002/ejic.201403140.
[3] Bhat GA, Rajendran A, Murugavel R. Dinuclear manganese(II), cobalt(II), and nickel(II) aryl phosphates incorporating 4′-chloro-2,2′:6′,2″-terpyridine coligands – efficient catalysts for alcohol oxidation. Eur J Inorg Chem 2018;2018:795–804. https://doi.org/10.1002/ejic.201701064.
[4] Wei C, He Y, Shi X, Song Z. Terpyridine-metal complexes: applications in catalysis and supramolecular chemistry. Coord Chem Rev 2019;385:1–19. https://doi.org/10.1016/j.ccr.2019.01.005.
[5] Cerfontaine S, Marcélis L, Laramee-Milette B, Hanan GS, Loiseau F, De Winter J, et al. Converging energy transfer in polynuclear Ru(II) multiterpyridine complexes: significant enhancement of luminescent properties. Inorg Chem 2018;57:2639–53. https://doi.org/10.1021/acs.inorgchem.7b03040.
[6] Polo AS, Itokazu MK, Murakami Iha NY. Metal complex sensitizers in dye-sensitized solar cells. Coord Chem Rev 2004;248:1343–61. https://doi.org/10.1016/j.ccr.2004.04.013.
[7] Duprez V, Biancardo M, Spanggaard H, Krebs FC. Synthesis of conjugated polymers containing Terpyridine−Ruthenium Complexes: photovoltaic applications. Macromolecules 2005;38:10436–48. https://doi.org/10.1021/ma051274f.
[8] Plenk C, Krause J, Rentschler E. A click-functionalized single-molecule magnet based on cobalt(II) and its analogous manganese(II) and zinc(II) compounds. Eur J Inorg Chem 2015;2015:370–4. https://doi.org/10.1002/ejic.201402955.
[9] Higgins RF, Livesay BN, Ozumerzifon TJ, Joyce JP, Rappé AK, Shores MP. A family of related Co(II) terpyridine compounds exhibiting field induced single-molecule magnet properties. Polyhedron 2018;143:193–200. https://doi.org/10.1016/j.poly.2017.10.008.
[10] Shi T, Xu Y, Li M-X, Liu C-M, Nfor EN, Wang Z-X. A 10-coordinate cerium(III) complex with a ferrocene-based terpyridine ligand exhibiting field-induced slow magnetic relaxation. Polyhedron 2020;188:114695. https://doi.org/10.1016/j.poly.2020.114695.
[11] Mondal D, Bar M, Maity D, Baitalik S. Anthraimidazoledione-terpyridine-based optical chemosensor for anions and cations that works as molecular half-subtractor, key-pad lock, and memory device. J Phys Chem C 2015;119:25429–41. https://doi.org/10.1021/acs.jpcc.5b08337.
[12] Hepp A, Ulrich G, Schmechel R, von Seggern H, Ziessel R. Highly efficient energy transfer to a novel organic dye in OLED devices. Synth Met 2004;146:11–5. https://doi.org/10.1016/j.synthmet.2004.06.016.
[13] Lakshmanan R, Shivaprakash NC, Sindhu S. Orange fluorescent Ru(III) complexes based on 4′-aryl substituted 2,2′:6′,2″-terpyridine for OLEDs application. J Fluoresc 2018;28:173–82. https://doi.org/10.1007/s10895-017-2180-5.
[14] Kumar A, Sun S-S, Lees AJ. Photophysics and photochemistry of organometallic rhenium diimine complexes. In: Lees AJ, editor. Photophysics of organometallics. Berlin, Heidelberg: Springer; 2010. p. 37–71. https://doi.org/10.1007/3418_2009_2.
[15] Chang K-C, Sun S-S, Lees AJ. Anion sensing by rhenium(I) carbonyls with polarized N–H recognition motifs. Inorg Chim Acta 2012;389:16–28. https://doi.org/10.1016/j.ica.2012.02.001.
[16] Lowe G, Droz AS, Vilaivan T, Weaver GW, Park JJ, Pratt JM, et al. Cytotoxicity of 2,2′:6′,2′ ‘-terpyridineplatinum(II) complexes against human ovarian carcinoma. J Med Chem 1999;42:3167–74. https://doi.org/10.1021/jm991053y.
[17] Qin Q-P, Wang Z-F, Wang S-L, Luo D-M, Zou B-Q, Yao P-F, et al. In vitro and in vivo antitumor activities of three novel binuclear platinum(II) complexes with 4′-substituted-2,2′:6′,2″-terpyridine ligands. Eur J Med Chem 2019;170:195–202. https://doi.org/10.1016/j.ejmech.2019.03.014.
[18] Altmann S, Choroba K, Skonieczna M, Zygadło D, Raczyńska-Szajgin M, Maroń A, et al. Platinum(II) coordination compounds with 4′-pyridyl functionalized 2,2′:6′,2″-terpyridines as an alternative to enhanced chemotherapy efficacy and reduced side-effects. J Inorg Biochem 2019;201:110809. https://doi.org/10.1016/j.jinorgbio.2019.110809.
[19] Rajalakshmi S, Weyhermüller T, Dinesh M, Nair BU. Copper(II) complexes of terpyridine derivatives: a footstep towards development of antiproliferative agent for breast cancer. J Inorg Biochem 2012;117:48–59. https://doi.org/10.1016/j.jinorgbio.2012.08.010.
[20] Naseri Z, Nemati Kharat A, Banavand A, Bakhoda A, Foroutannejad S. First row transition metal complexes of thienyl substituted terpyridine: structural, photophysical and biological studies. Polyhedron 2012;33:396–403. https://doi.org/10.1016/j.poly.2011.11.060.
[21] Wang S, Chu W, Wang Y, Liu S, Zhang J, Li S, et al. Synthesis, characterization and cytotoxicity of Pt(II), Pd(II), Cu(II) and Zn(II) complexes with 4’-substituted terpyridine. Appl Organomet Chem 2013;27:373–9. https://doi.org/10.1002/aoc.2988.
[22] Eryazici I, Moorefield CN, Newkome GR. Square-planar Pd(II), Pt(II), and Au(III) terpyridine complexes: their syntheses, physical properties, supramolecular constructs, and biomedical activities. Chem Rev 2008;108:1834–95. https://doi.org/10.1021/cr0781059.
[23] Mughal EU, Mirzaei M, Sadiq A, Fatima S, Naseem A, Naeem N, et al. Terpyridine-metal complexes: effects of different substituents on their physico-chemical properties and density functional theory studies, vol. 7. Royal Society Open Science; 2012. https://doi.org/10.1098/rsos.201208. 08.
[24] Abel EW, Dimitrov VS, Long NJ, Orrell KG, Osborne AG, Pain HM, et al. 2,2′:6′,2″-Terpyridine (terpy) acting as a fluxional bidentate ligand. Part 2. Rhenium carbonyl halide complexes, fac-[ReX(CO)3(terpy)](X = Cl, Br or I): NMR studies of their solution dynamics, synthesis of cis-[ReBr(CO)2(terpy)] and the crystal structure of [ReBr(CO)3(terpy)]. J Chem Soc, Dalton Trans 1993:597–603. https://doi.org/10.1039/DT9930000597.
[25] Ghosh BN, Topić F, Sahoo PK, Mal P, Linnera J, Kalenius E, et al. Synthesis, structure and photophysical properties of a highly luminescent terpyridine-diphenylacetylene hybrid fluorophore and its metal complexes. Dalton Trans 2014;44:254–67. https://doi.org/10.1039/C4DT02728K.
[26] Ghosh BN, Lahtinen M, Kalenius E, Mal P, Rissanen K. 2,2′:6′,2″-Terpyridine trimethylplatinum(IV) iodide complexes as bifunctional halogen bond acceptors. Cryst Growth Des 2016;16:2527–34. https://doi.org/10.1021/acs.cgd.5b01552.
[27] Ghosh BN, Puttreddy R, Rissanen K. Synthesis and structural characterization of new transition metal complexes of a highly luminescent amino-terpyridine ligand. Polyhedron 2020;177:114304. https://doi.org/10.1016/j.poly.2019.114304.

[28] Amoroso A J, Banu A, Coogan M P, Edwards P G, Hossain G, Abdul Malik KM. Functionalisation of terpyridine complexes containing the Re(CO)3+ moiety. Dalton Trans 2010;39:6993–7003. https://doi.org/10.1039/C0DT00174K.

[29] Klemens T, Świtlicka-Olszewska A, Machura B, Grucela M, Schab-Balcerzak E, Smolarek K, et al. Rhenium(I) terpyridine complexes – synthesis, photophysical properties and application in organic light emitting devices. Dalton Trans 2016;45:1746–62. https://doi.org/10.1039/C5DT04093K.

[30] Klemens T, Świtlicka-Olszewska A, Machura B, Grucela M, Janeczek H, Schab-Balcerzak E, et al. Synthesis, photophysical properties and application in organic light emitting devices of rhenium(I) carbonyls incorporating functionalized 2,2′:6′,2″-terpyridines. RSC Adv 2016;6:56335–52. https://doi.org/10.1039/C6RA08981J.

[31] Klemens T, Świtlicka A, Machura B, Kula S, Krompiec S, Łaba K, et al. A family of solution processable ligands and their Re(I) complexes towards light emitting applications. Dyes Pigments 2019;163:86–101. https://doi.org/10.1016/j.dyepig.2018.11.035.

[32] Klemens T, Czerwińska K, Szlapa-Kula A, Kula S, Świtlicka A, Kotowicz S, et al. Synthesis, spectroscopic, electrochemical and computational studies of rhenium(I) tricarbonyl complexes based on bidentate-coordinated 2,6-di(thiazol-2-yl)pyridine derivatives. Dalton Trans 2017;46:9605–20. https://doi.org/10.1039/C7DT01948C.

[33] Klemens T, Świtlicka A, Kula S, Siwy M, Łaba K, Grzelak J, et al. The effect of 2-, 3- and 4-pyridyl substituents on photophysics of fac-[ReCl(CO)3(n-pytpy-κ2N)] complexes: experimental and theoretical insights. J Lumin 2019;209:346–56. https://doi.org/10.1016/j.jlumin.2019.01.045.

[34] Abel EW, Long NJ, Orrell KG, Osborne AG, Pain HM, Šik V. The first examples of 2,2′:6′,2″-terpyridine as a fluxional bidentate ligand. J Chem Soc, Chem Commun 1992;303–4. https://doi.org/10.1039/C39920000303.

[35] Vitvarová T, Zedník J, Bláha M, Vohlídal J, Svoboda J. Effect of ethynyl and 2-thienyl substituents on the complexation of 4′-substituted 2,2′:6′,2″-terpyridines with Zn2+ and Fe2+ ions, and the spectroscopic properties of the ligands and formed complex species. Eur J Inorg Chem 2012;2012:3866–74. https://doi.org/10.1002/ejic.201200256.

[36] McMillin DR, Moore JJ. Luminescence that lasts from Pt(trpy)Cl+ derivatives (trpy=2,2′;6′,2″-terpyridine). Coord Chem Rev 2002;229:113–21. https://doi.org/10.1016/S0010-8545(02)00041-3.

[37] Crites DK, Cunningham CT, McMillin DR. Remarkable substituent effects on the photophysics of Pt(4′-X-trpy)Cl+ systems (trpy = 2,2′; 6′,2″-terpyridine). Inorg Chim Acta 1998;273:346–53. https://doi.org/10.1016/S0020-1693(97)06082-9.

[38] Genoni A, Chirdon DN, Boniolo M, Sartorel A, Bernhard S, Bonchio M. Tuning iridium photocatalysts and light irradiation for enhanced CO2 reduction. ACS Catal 2017;7:154–60. https://doi.org/10.1021/acscatal.6b03227.

[39] Meudtner RM, Ostermeier M, Goddard R, Limberg C, Hecht S. Multifunctional "clickates" as versatile extended heteroaromatic building blocks: efficient synthesis via click chemistry, conformational preferences, and metal coordination. Chem Eur J 2007;13:9834–40. https://doi.org/10.1002/chem.200701240.

[40] Cabrero-Antonino M, Ballesteros-Garrido R, Chiassai L, Escrivà E, Arellano CR de, Ballesteros R, et al. Synthesis of new terpyridine-like ligands based on triazolopyridines and benzotriazoles. New J Chem 2017;41:4918–22. https://doi.org/10.1039/C7NJ00962C.

[41] Halcrow MA. The synthesis and coordination chemistry of 2,6-bis(pyrazolyl)pyridines and related ligands — versatile terpyridine analogues. Coord Chem Rev 2005;249:2880–908. https://doi.org/10.1016/j.ccr.2005.03.010.

[42] Attwood M, Turner SS. Back to back 2,6-bis(pyrazol-1-yl)pyridine and 2,2′:6′,2″-terpyridine ligands: untapped potential for spin crossover research and beyond. Coord Chem Rev 2017;353:247–77. https://doi.org/10.1016/j.ccr.2017.09.025.

[43] Cook LJK, Tuna F, Halcrow M A. Iron(ii) and cobalt(ii) complexes of tris-azinyl analogues of 2,2′:6′,2″-terpyridine. Dalton Trans 2013;42:2254–65. https://doi.org/10.1039/C2DT31736B.

[44] Desimoni G, Faita G, Quadrelli P. Pyridine-2,6-bis(oxazolines), helpful ligands for asymmetric catalysts. Chem Rev 2003;103:3119–54. https://doi.org/10.1021/cr020004h.

[45] Boča M, Jameson RF, Linert W. Fascinating variability in the chemistry and properties of 2,6-bis-(benzimidazol-2-yl)-pyridine and 2,6-bis-(benzthiazol-2-yl)-pyridine and their complexes. Coord Chem Rev 2011;255:290–317. https://doi.org/10.1016/j.ccr.2010.09.010.

[46] Choroba K, Kula S, Maroń A, Machura B, Małecki J, Szłapa-Kula A, et al. Aryl substituted 2,6-di(thiazol-2-yl)pyridines –excited-state characterization and potential for OLEDs. Dyes Pigments 2019;169:89–104. https://doi.org/10.1016/j.dyepig.2019.05.015.

[47] Yin Z, Zhang G, Phoenix T, Zheng S, Fettinger J C. Assembling mono-, di- and tri-nuclear coordination complexes with a ditopic analogue of 2,2′:6′,2″-terpyridine: syntheses, structures and catalytic studies. RSC Adv 2015;5:36156–66. https://doi.org/10.1039/C5RA06197K.

[48] Krishna A, Darshan V, Suresh CH, Narayanan Unni KN, Varma RL. Solution processable carbazole derivatives for dopant free single molecule white electroluminescence by room temperature phosphorescence. J Photochem Photobiol Chem 2018;360:249–54. https://doi.org/10.1016/j.jphotochem.2018.04.038.

[49] Kong M, Liu Y, Wang H, Luo J, Li D, Zhang S, et al. Synthesis, spectral and third-order nonlinear optical properties of terpyridine Zn(II) complexes based on carbazole derivative with polyether group. Spectrochim Acta Mol Biomol Spectrosc 2015;135:521–8. https://doi.org/10.1016/j.saa.2014.07.039.

[50] Chen X, Zhou Q, Cheng Y, Geng Y, Ma D, Xie Z, et al. Synthesis, structure and luminescence properties of zinc (II) complexes with terpyridine derivatives as ligands. J Lumin 2007;126:81–90. https://doi.org/10.1016/j.jlumin.2006.05.008.

[51] Hwang S-H, Wang P, Moorefield CN, Godínez LA, Manríquez J, Bustos E, et al. Design, self-assembly, and photophysical properties of pentameric metallomacrocycles: [M5(N-hexyl[1,2-bis(2,2′:6′,2″-terpyridin-4-yl)]carbazole)5] [M = Fe(II), Ru(II), and Zn(II)]. Chem Commun 2005:4672–4. https://doi.org/10.1039/B509662F.

[52] Choroba K, Maroń A, Świtlicka A, Szłapa-Kula A, Siwy M, Grzelak J, et al. Carbazole effect on ground- and excited-state properties of rhenium(I) carbonyl complexes with extended terpy-like ligands. Dalton Trans 2021;50:3943–58. https://doi.org/10.1039/D0DT04340K.

[53] Baschieri A, Sambri L, Gualandi I, Tonelli D, Monti F, Esposti AD, et al. Carbazole-terpyridine donor–acceptor luminophores. RSC Adv 2013;3:6507–17. https://doi.org/10.1039/C3RA23380D.

[54] Dahule HK, Thejokalyani N, Dhoble SJ. Novel Br-DPQ blue light-emitting phosphors for OLED. Luminescence 2015;30:405–10. https://doi.org/10.1002/bio.2750.

[55] Hsu M-A, Chow TJ. Light emitting materials and devices of PPV type compounds containing quinolines. J Chin Chem Soc 2005;52:811–8. https://doi.org/10.1002/jccs.200500114.

[56] Toledo D, Brovelli F, Soto-Delgado J, Peña O, Pivan J-Y, Moreno Y. Influence of structural changes on photophysical properties of terpyridine derivates: experimental studies and theoretical calculations. J Mol Struct 2018;1153:282–91. https://doi.org/10.1016/j.molstruc.2017.10.011.

[57] Toledo D, Vega A, Pizarro N, Baggio R, Peña O, Roisnel T, et al. Comparitive study on structural, magnetic and spectroscopic properties of four new copper(II) coordination polymers with 4′-substituted terpyridine ligands. J Solid State Chem 2017;253:78–88. https://doi.org/10.1016/j.jssc.2017.05.017.

[58] Toledo D, Baggio R, Freire E, Vega A, Pizarro N, Moreno Y. Structure and spectroscopy of two new bases for building block: terpyridine derivatives. J Mol Struct 2015;1102:18–24. https://doi.org/10.1016/j.molstruc.2015.08.030.

[59] Lewandowska A, Wróblewski D, Guzow K, Milewska M, Czaplewski C, Wiczk W. Acid-base properties of 3-[2-(n-quinolinyl)benzoxazol-5-yl]alanine derivatives in the ground and excited state. Experimental and theoretical studies. J Photochem Photobiol Chem 2018;353:191–9. https://doi.org/10.1016/j.jphotochem.2017.11.017.

[60] Maroń A, Szlapa A, Klemens T, Kula S, Machura B, Krompiec S, et al. Tuning the photophysical properties of 4′-substituted terpyridines – an experimental and theoretical study. Org Biomol Chem 2016;14:3793–808. https://doi.org/10.1039/C6OB00038J.

[61] Maroń A, Kula S, Szlapa-Kula A, Świtlicka A, Machura B, Krompiec S, et al. 2,2′:6′,2″-Terpyridine analogues: structural, electrochemical, and photophysical properties of 2,6-Di(thiazol-2-yl)pyridine derivatives. Eur J Org Chem 2017;2017:2730–45. https://doi.org/10.1002/ejoc.201700141.

[62] Czerwińska K, Machura B, Kula S, Krompiec S, Erfurt K, Roma-Rodrigues C, et al. Copper(II) complexes of functionalized 2,2′:6′,2″-terpyridines and 2,6-di(thiazol-2-yl)pyridine: structure, spectroscopy, cytotoxicity and catalytic activity. Dalton Trans 2017;46:9591–604. https://doi.org/10.1039/C7DT01244F.

[63] Palion-Gazda J, Machura B, Klemens T, Szlapa-Kula A, Krompiec S, Siwy M, et al. Structure-dependent and environment-responsive optical properties of the trisheterocyclic systems with electron donating amino groups. Dyes Pigments 2019;166:283–300. https://doi.org/10.1016/j.dyepig.2019.03.035.

[64] Szlapa-Kula A, Małecka M, Machura B. Insight into structure-property relationships of aryl-substituted 2,2′:6′,2″-terpyridines. Dyes Pigments 2020;180:108480. https://doi.org/10.1016/j.dyepig.2020.108480.

[65] CrysAlis. Pro. Yarnton, England: Oxford Diffraction Ltd; 2011.

[66] Sheldrick GM. A short history of SHELX. Acta Crystallogr A 2008;64:112–22. https://doi.org/10.1107/S0108767307043930.

[67] Sheldrick GM. Crystal structure refinement with SHELXL. Acta Crystallogr C 2015;71:3–8. https://doi.org/10.1107/S2053229614024218.

[68] Slavov C, Hartmann H, Wachtveitl J. Implementation and evaluation of data analysis strategies for time-resolved optical spectroscopy. Anal Chem 2015;87:2328–36. https://doi.org/10.1021/ac504348h.

[69] Frisch MJ, Trucks GW, Cheeseman JR, Scalmani G, Caricato M, Hratchian HP, et al. Gaussian 09. n.d.

[70] Perdew JP, Burke K, Ernzerhof M. Generalized gradient approximation made simple. Phys Rev Lett 1996;77:3865–8. https://doi.org/10.1103/PhysRevLett.77.3865.

[71] Adamo C, Barone V. Toward reliable density functional methods without adjustable parameters: the PBE0 model. J Chem Phys 1999;110:6158–70. https://doi.org/10.1063/1.478522.

[72] Weigend F, Ahlrichs R. Balanced basis sets of split valence, triple zeta valence and quadruple zeta valence quality for H to Rn: design and assessment of accuracy. Phys Chem Chem Phys 2005;7:3297–305. https://doi.org/10.1039/B508541A.

[73] Rappoport D, Furche F. Property-optimized Gaussian basis sets for molecular response calculations. J Chem Phys 2010;133:134105. https://doi.org/10.1063/1.3484283.

[74] Andrae D, Häußermann U, Dolg M, Stoll H, Preuß H. Energy-adjustedab initio pseudopotentials for the second and third row transition elements. Theor Chim Acta 1990;77:123–41. https://doi.org/10.1007/BF01114537.

[75] Cancès E, Mennucci B, Tomasi J. A new integral equation formalism for the polarizable continuum model: theoretical background and applications to isotropic and anisotropic dielectrics. J Chem Phys 1997;107:3032–41. https://doi.org/10.1063/1.474659.

[76] Mennucci B, Tomasi J. Continuum solvation models: a new approach to the problem of solute's charge distribution and cavity boundaries. J Chem Phys 1997;106:5151–8. https://doi.org/10.1063/1.473558.

[77] Cossi M, Barone V, Mennucci B, Tomasi J. Ab initio study of ionic solutions by a polarizable continuum dielectric model. Chem Phys Lett 1998;286:253–60. https://doi.org/10.1016/S0009-2614(98)00106-7.
[78] Suntrup L, Klenk S, Klein J, Sobottka S, Sarkar B. Gauging donor/acceptor properties and redox stability of chelating click-derived triazoles and triazolylidenes: a case study with rhenium(I) complexes. Inorg Chem 2017;56:5771–83. https://doi.org/10.1021/acs.inorgchem.7b00393.
[79] Bujak P, Kulszewicz-Bajer I, Zagorska M, Maurel V, Wielgus I, Pron A. Polymers for electronics and spintronics. Chem Soc Rev 2013;42:8895–999. https://doi.org/10.1039/C3CS60257E.
[80] Małecka M, Machura B, Świtlicka A, Kotowicz S, Szafraniec-Gorol G, Siwy M, et al. Towards better understanding of photophysical properties of rhenium(I) tricarbonyl complexes with terpy-like ligands. Spectrochim Acta Mol Biomol Spectrosc 2020;231:118124. https://doi.org/10.1016/j.saa.2020.118124.
[81] Wang D, Xu Q-L, Zhang S, Li H-Y, Wang C-C, Li T-Y, et al. Synthesis and photoluminescence properties of rhenium(I) complexes based on 2,2′:6′,2″-terpyridine derivatives with hole-transporting units. Dalton Trans 2013;42:2716–23. https://doi.org/10.1039/C2DT32154H.
[82] Juris A, Campagna S, Bidd I, Lehn JM, Ziessel R. Synthesis and photophysical and electrochemical properties of new halotricarbonyl(polypyridine)rhenium(I) complexes. Inorg Chem 1988;27:4007–11. https://doi.org/10.1021/ic00295a022.
[83] Fernández-Terán R, Sévery L. Living long and prosperous: productive intraligand charge-transfer states from a rhenium(I) terpyridine photosensitizer with enhanced light absorption. Inorg Chem 2020. https://doi.org/10.1021/acs.inorgchem.0c01939.
[84] Sousa S F, Sampaio R N, Neto NMB, Machado AE H, Patrocinio AO T. The photophysics of fac -[Re(CO) 3 (NN)(bpa)] + complexes: a theoretical/experimental study. Photochem Photobiol Sci 2014;13:1213–24. https://doi.org/10.1039/C4PP00074A.
[85] Ramos LD, Sampaio RN, Assis FF de, Oliveira KT de, Homem-de-Mello P, Patrocinio AOT, et al. Contrasting photophysical properties of rhenium(I) tricarbonyl complexes having carbazole groups attached to the polypyridine ligand. Dalton Trans 2016;45:11688–98. https://doi.org/10.1039/C6DT01112H.
[86] Maroń A M, Szlapa-Kula A, Matussek M, Kruszynski R, Siwy M, Janeczek H, et al. Photoluminescence enhancement of Re(i) carbonyl complexes bearing D–A and D–π–A ligands. Dalton Trans 2020;49:4441–53. https://doi.org/10.1039/C9DT04871E.
[87] El Nahhas A, Cannizzo A, van Mourik F, Blanco-Rodríguez AM, Záliš S, Vlček A, et al. Ultrafast excited-state dynamics of [Re(L)(CO)3(bpy)] n complexes: involvement of the solvent. J Phys Chem 2010;114:6361–9. https://doi.org/10.1021/jp101999m.
[88] El Nahhas A, Consani C, Blanco-Rodríguez AM, Lancaster KM, Braem O, Cannizzo A, et al. Ultrafast excited-state dynamics of rhenium(I) photosensitizers [Re(Cl)(CO)3(N,N)] and [Re(imidazole)(CO)3(N,N)]+: diimine effects. Inorg Chem 2011;50:2932–43. https://doi.org/10.1021/ic102324p.
[89] Ragazzon G, Verwilst P, Denisov SA, Credi A, Jonusauskas G, McClenaghan ND. Ruthenium(II) complexes based on tridentate polypyridine ligands that feature long-lived room-temperature luminescence. Chem Commun 2013;49:9110–2. https://doi.org/10.1039/C3CC45387A.

Abbreviations

bipy: 2,2′-bipyridine
DAS: decay associated spectra
dppy: 2,6-di(pyrazin-2-yl)pyridine
dtpy: 2,6-di(thiazol-2-yl)pyridine
EA: electron affinity
EL: electroluminescence
em: emission
ESA: excited-state absorption
ex: excitation
fsTA: femtosecond transient absorption
GLA: global lifetime analysis
IP: ionization potential
IRF: instrument response function
ISC: inter-system crossing
ITO: indium-tin oxide
MCS: multi-channel scaling
PBD: 2-(4-tert-butylphenyl)-5-(4-biphenylyl)-1,3,4-oxadiazole
PCM: polarizable continuum model
PEDOT: poly(3,4-(ethylenedioxy)thiophene)
PL: photoluminescence
PSS: poly-(styrenesulfonate)
PVK: poly(9-vinylcarbazole)
TA: transient absorption
TCSPC: time correlated single photon counting
terpy2,2′:: 6′,2″-terpyridine